Modes of rifting in magma-rich settings: Tectono-magmatic evolution of Central Afar

Martin Stab, Nicolas Bellahsen, Raphaël Pik, Xavier Quidelleur, Dereje Ayalew, Sylvie Leroy

AGU PUBLICATIONS

Tectonics

RESEARCH ARTICLE
10.1002/2015TC003893

Modes of rifting in magma-rich settings: Tectono-magmatic evolution of Central Afar

Martin Stab[1,2], Nicolas Bellahsen[1], Raphaël Pik[2], Xavier Quidelleur[3,4], Dereje Ayalew[5], and Sylvie Leroy[1]

[1]Sorbonne Universités, UPMC Université Paris 06, CNRS, Institut des Sciences de la Terre de Paris (iSTeP), Paris, France, [2]CRPG UMR 7358 CNRS, Université de Lorraine, Nancy, France, [3]Université Paris-Sud, Laboratoire GEOPS, UMR 8148, Orsay, France, [4]CNRS, Orsay, France, [5]School of Earth Sciences, Addis Ababa University, Addis Ababa, Ethiopia

Key Points:
- Divergence during the Mio-Pliocene is diffuse (magmatic wide rift)
- Central Afar lower crust has been rethickened by magmatic underplating
- Shear zones at midcrustal levels may accommodate extension

Correspondence to:
M. Stab,
mstab@crpg.cnrs-nancy.fr

Citation:
Stab, M., N. Bellahsen, R. Pik, X. Quidelleur, D. Ayalew, and S. Leroy (2016), Modes of rifting in magma-rich settings: Tectono-magmatic evolution of Central Afar, *Tectonics*, *35*, 2–38, doi:10.1002/2015TC003893.

Received 23 MAR 2015
Accepted 4 OCT 2015
Accepted article online 8 OCT 2015
Published online 6 JAN 2016

Abstract Recent research in Afar (northern Ethiopia) has largely focused on the formation of the present-day ocean-continent transition at active segments (e.g., Manda Hararo). However, the Oligo-Miocene history of extension, from the onset of rifting at ~25 Ma to the eruption of the massive Stratoïd flood basalts at ~4 Ma, remains poorly constrained. Here we present new structural data and radiometric dating from Central Afar, obtained along a zone stretching from the undeformed Oligocene Ethiopian plateau to the Manda Hararo and Tat'Ale active volcanic segments. Basaltic and rhyolitic formations were mapped in two key areas corresponding to the proximal and distal parts of a half-rift. We present a balanced composite cross section of Central Afar, reconstructed using our new data and previously published geophysical data on the crustal structure. Our main findings are as follows: (1) Extension during the Mio-Pliocene corresponds to a "wide rift" style of rifting. (2) The lower crust has been underplated/intruded and rethickened during rifting by magmatic injection. (3) Our restoration points to the existence of midcrustal shear zones that have helped to distribute extension in the upper crust and to localize extension at depth in a necking zone. Moreover, we suggest that there is a close relationship between the location of a shear zone and the underplated/intruded material. In magma-rich environments such as Central Afar, breakup should be achieved once the initial continental crust has been completely replaced by the newly, magmatically accreted crust. Consequently, and particularly in Afar, crustal thickness is not necessarily indicative of breakup but instead reflects differences in tectono-magmatic regimes.

1. Introduction

Magmatism and extensional processes are fundamental to our understanding of the formation of rift basins and their potential evolution into continental passive margins and therefore tectonic plate boundaries. Interactions between tectonics and magmatism have been investigated at all scales, from the geodynamic reconstruction of plate motions to mid-oceanic ridges. The relationship between magma supply and continental extension (rifting) has received much attention. For example, localized magmatism can help focus extension [*Buck*, 1991; *Ebinger et al.*, 2013], whereas disperse magmatism appears to distribute extension [*Corti et al.*, 2003], magma supply can facilitate rifting of the lithosphere in the absence of sufficient tectonic force [*Buck*, 2004, 2006], and dyking and underplating appear to accommodate divergence without involving significant normal faulting [i.e., *Grandin et al.*, 2010]. Thus, tectono-magmatic interactions play a significant role in shaping rift basins and rifted passive margins. Given the various rift structures documented in the literature, it is essential to improve our understanding of rheology, i.e., the structural and thermal evolution of the lithosphere. The simple idea of stretching and thinning a lithosphere to 0 km [*McKenzie*, 1978] no longer holds as geological observations made in the past few decades have highlighted a considerable degree of complexity. Rifts may be narrow or wide and magma-poor or magma-rich, and the lithosphere may initially be thin and hot or old and cold [e.g., *Buck*, 1991; *Brun*, 1999]. While analog and numerical simulations can handle many of these rheological parameters and therefore provide important constraints on rifting processes, the effects of magma supply on rheology, and hence on the structural style of a passive margin, remain largely unknown.

Magmatism at nascent passive margins is dependent on the state of the underlying mantle. In Large Igneous Provinces (LIP), the huge eruptions of Continental Flood Basalts (CFB) are commonly related to mantle-scale thermal anomalies known as mantle plumes. The origin of mantle plumes is a subject of intense debate in the literature and will not be discussed in this paper. Nevertheless, mantle plumes are thermal anomalies,

sometimes originating from the deep mantle, that trigger adiabatic melting and bring magma to the surface. The existence of such thermal anomalies may be unrelated to any other preexisting tectonic process in continental [*Courtillot et al*., 1999] and more often in oceanic settings [*Le Bas*, 1987]. As such, plumes could be a prerift feature [*Courtillot et al*., 1999; *Hofmann et al*., 1997] or they may be superimposed on the earlier tectonic history [*Ziegler et al*., 2001; *Nikishin et al*., 2002; *Ziegler and Cloetingh*, 2004; *Geoffroy*, 2005]. In volcanic passive margins, the eruption of massive flood basalt prisms, tilting toward the ocean and controlled by continent-facing normal faults (the so-called seaward dipping reflectors or SDR), is related to the syn-rift or the syn-breakup history of the margin [*Hinz*, 1981; *Mutter et al*., 1982; *Coffin and Eldholm*, 1994; *Menzies et al*., 2002; *Geoffroy*, 2005; *Franke*, 2013; *Quirk et al*., 2014]. This raises the question of whether magmatism during margin development necessitates the existence of a plume-type thermal anomaly or if it might instead be the consequence of processes related to lithospheric thinning, such as adiabatic decompression [*Van Wijk et al*., 2001], small-scale convection in the mantle [*Anderson*, 1994; *Huismans et al*., 2001; *Ballmer et al*., 2007], lateral rifting diachronism controlled by transform zones [*Koopmann et al*., 2014], pre-CFB thinning [*Armitage et al*., 2009], or modification of the mantle's fertility by delamination [e.g., *Anderson*, 2005]. A margin can sometimes be of sedimentary rather than volcanic nature, even if it is located close to a contemporaneous CFB province at the time of rifting [*Franke*, 2013]. There therefore appears to be a complex spatial and temporal relationship between plume-generated magmatic provinces and volcanic passive margins, and the simple notion of purely "active" and "passive" rifting of *Sengör and Burke* [1978] can no longer be applied in explanations of margin formation.

Volcanic passive margins should therefore be considered in the context of their main two, closely related, features. (1) The first of these are the tectonic structures. Extension and thinning of the lithosphere is recorded by syn-rift structures, such as tilted blocks in the proximal margin and detachments in the most distal parts that, along with the SDR, form the ocean-continent transition (OCT) [*Péron-Pinvidic et al*., 2013]. These two types of structural feature are well documented at magma-poor margins and in continental rifts and are linked to the tectonic history. (2) The second key feature of the volcanic passive margin is magmatism. Magmatic activity at volcanic passive margins is expressed by the eruption of CFB and emplacement of SDR. These are sometimes superimposed on an earlier phase of tectonic activity and associated with high velocity lower crust imaged by seismic refraction, seismology, gravimetry, and magnetism [e.g., *Ahmed et al*., 2013]. This high velocity lower crust is primarily interpreted, among other possibilities, as mafic underplating of the thinned crust [*White et al*., 2008; *Thybo and Nielsen*, 2009; *Thybo and Artemieva*, 2013]. Extrusive and intrusive magmatism both constitute new transitional crust, which is commonly observed in geophysical studies [*Holbrook et al*., 2001; *White et al*., 2008; *Mjelde et al*., 2009; *Voss et al*., 2009; *Thybo and Nielsen*, 2009]. However, investigating the transitional crust involves further issues. First, the SDR commonly act as an observational mask in geophysics. Seismic waves are often reflected on the SDR, making it impossible to observe the underlying OCT-related structures. Second, the accretion of transition crust during rifting involves a certain degree of syn-rift magma-compensated thinning, making it difficult to establish a sound balanced cross section [*Geoffroy*, 2005]. Thus, a current issue regarding volcanic passive margins is to be able to distinguish between tectonic stretching and thinning and magmatic underplating. Third, the rheological effects of magmatic underplating remain poorly constrained.

To address these three key issues, we have investigated extension and magmatism in the Afar Depression—a magmatic rift that has not yet reached the breakup stage. This locality presents several advantages, in particular the fact that there are no thick volcanics masking the syn-rift structures because the rift has not yet reached breakup (although it is probably close to it [see *Hammond et al*., 2011]). The Afar Depression extends from the Ethiopian plateau to the magmatic active segments that define the plate boundary between the Nubian and Arabian plates (Figure 1). Rifting in Afar began during the Oligocene, soon after the impingement of the Afar mantle plume and the subsequent eruption of the Ethiopian large igneous province at around 30 Ma [*Hofmann et al*., 1997]. Seismic studies show the presence of a broad mantle anomaly rooted at the core-mantle boundary [*Ritsema and Allen*, 2003; *Simmons et al*., 2007; *Bastow et al*., 2008; *Li et al*., 2008; *Ritsema et al*., 2011], and the Afar rift is therefore considered an example of rifting following impingement of a plume-like thermal anomaly. The Afar rift system (Figure 1) has been interpreted as an asymmetric rift, analogous to SDR, where strain and magmatism have migrated toward the rift center and play a major role in dyking [*Ebinger and Casey*, 2001; *Wolfenden et al*., 2005], or alternatively, as a detachment-dominated rift [*Ghebreab and Talbot*, 2000; *Geoffroy et al*., 2014]. The relationship between normal faulting, dyking, and low-angle faults therefore remains unclear.

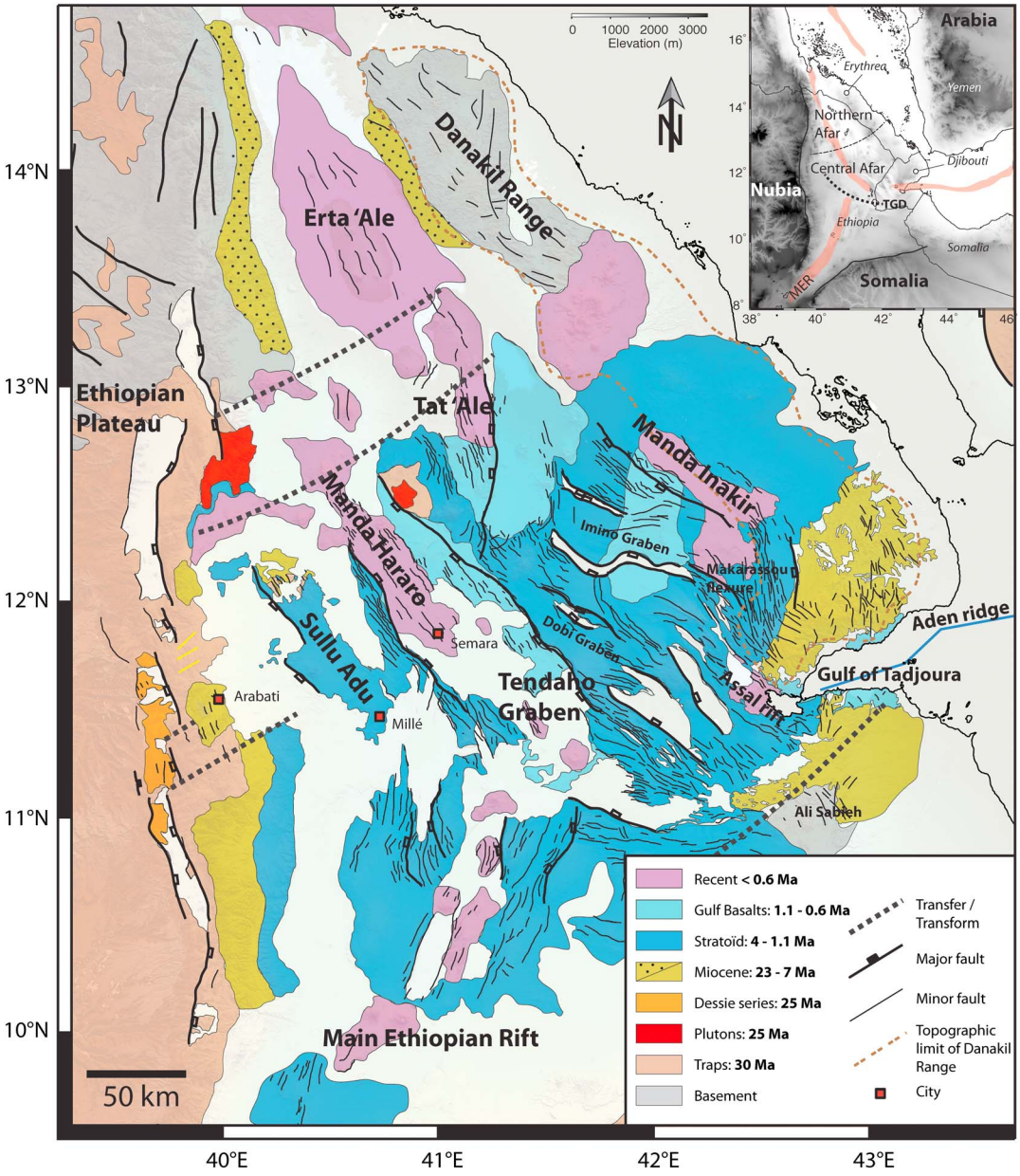

Figure 1. Structural map of the Afar Depression, modified from *Varet* [1978] and *Wolfenden et al.* [2005] for the southwestern marginal part (south of Arabati), from *Le Gall* [2014] for Djibouti, and from *Kidane et al.* [2003] for Tendaho Graben. Datum: WGS84. Grey = basement rocks (undifferentiated, crystalline, or cretaceous limestones). Brown = Traps series, prerift. Red = plutonic/ intrusive rock (Limmo massif and Affara Dara massif, see Figure 2a). The orange unit (Dessie series) is defined as the circa 25 Ma basaltic series found in the present-day marginal graben and absent in the Afar depression, documented by *Ukstins et al.* [2002]. The yellow unit, labeled "Miocene," represents the volcanic sequence described in this study, as well as other Miocene formations (e.g., the Mabla and Dahla Formations, Djibouti). The dotted yellow unit in the Erta'Ale segment represents the Red Beds series [*Varet*, 1978], which are sedimentary deposits, possibly Miocene in age. The blue unit is the mainly basaltic Stratoïd Formation, whereas the light blue unit corresponds to the Gulf Basalts as redefined by *Kidane et al.* [2003]. Recent lavas are restricted to active segments and are shown in purple. Quaternary infill is shown white. See text for more details of the volcano-stratigraphy. The grey dotted lines are transform. The thick dotted line is the Tendaho Goba'ad Discontinuity (TGD), which marks the change from Red Sea-oriented to MER-oriented structures [*Harding et al.*, 1990; *Hayward and Ebinger*, 1996]. The thin brown double-dotted line represents the contour of the Danakil block as described in the literature [*Eagles et al.*, 2002]. Major faults are defined as faults with throws >100 m.

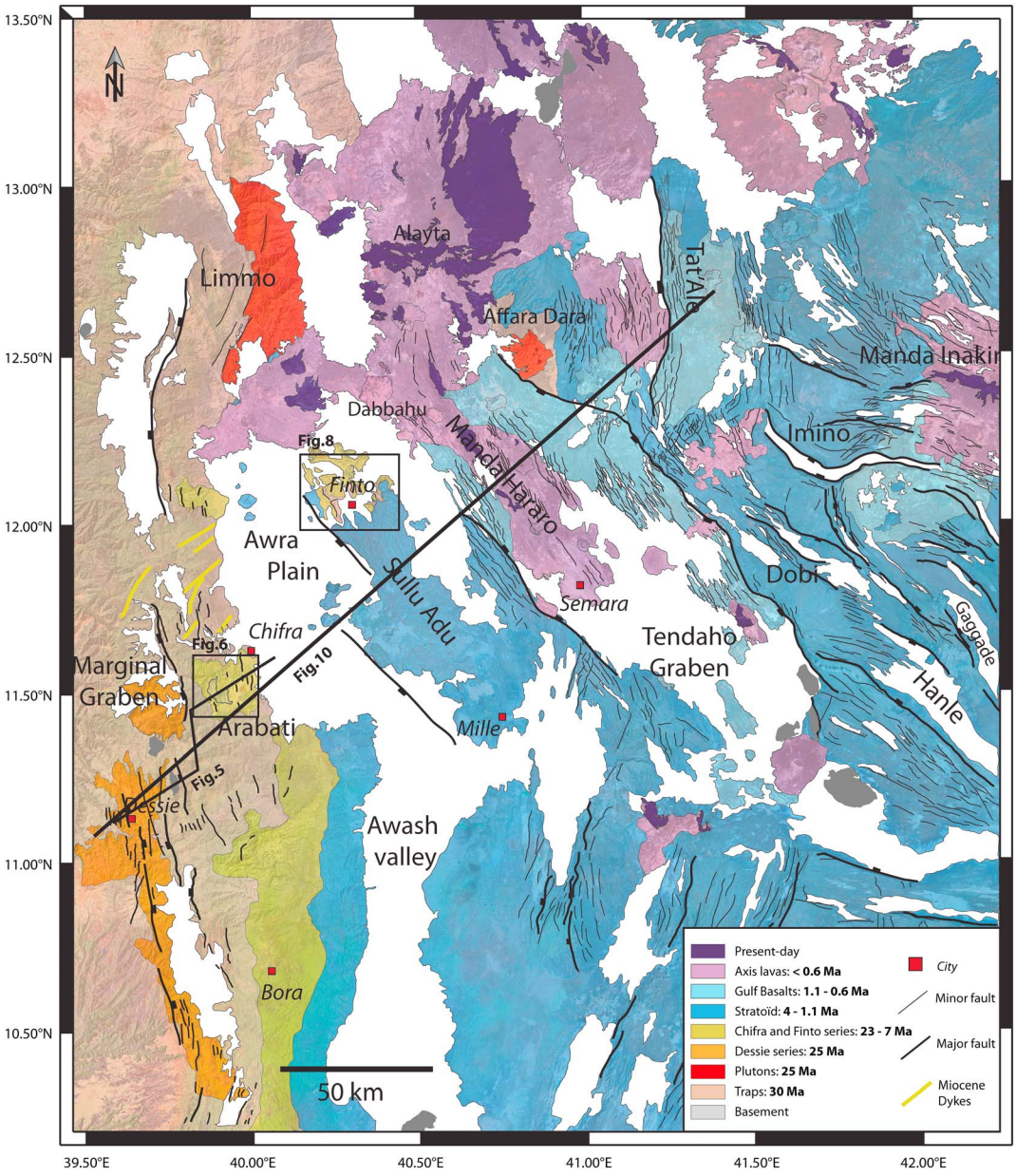

Figure 2. (a) Zoom on the Central Afar, Ethiopia. Datum WGS84, projection UTM 37°N. Same color code as used in Figure 1. Structures mainly trend NW-SE in the study area, so the area investigated is a near-cylindrical half-rift. Black rectangles outline the two key study areas (Arabati, Figure 6; Sullu Adu, Figure 8). The thin black line (labeled Figure 5) indicates the location of the Arabati cross section. The thick black line marks the NE-SW trending composite cross section (Figure 10). Note the overall SW dip of major faults. (b) Compilation of age data from the literature and from this study (same area as Figure 2a). Ages (in Ma) were mostly determined by K-Ar and Ar/Ar methods, except for data from this study ((U-Th-Sm)/He and K-Ar). See legend for sources of published ages. WR = Whole Rock age (analysis was not performed on separated minerals). Although WR ages should be treated with caution, they nevertheless show a good agreement with more recently published data. Ages shown of Figure 2b are from *Kunz et al.* [1975], *Barberi et al.* [1975], *Zumbo et al.* [1995], *Lahitte et al.* [2001, 2003a, 2003b], *Ukstins et al.* [2002], *Coulié* [2001], *Coulié et al.* [2003], *Wolfenden et al.* [2005], and this study.

We present new structural observations and mapping, along with (U-Th-Sm)/He and K-Ar ages of the volcanic record of Central Afar. We use this new set of data alongside published geophysical data (receiver functions and wide-angle controlled source imaging) to construct a composite balanced cross section of Central Afar, stretching from the Ethiopian Plateau in the west to the active segments of Manda Hararo and Tat'Ale (Figure 1). We document the extension and thinning of this rift segment and then discuss their significance in the light of relevant observations about the state of the mantle from previous studies in order to unravel

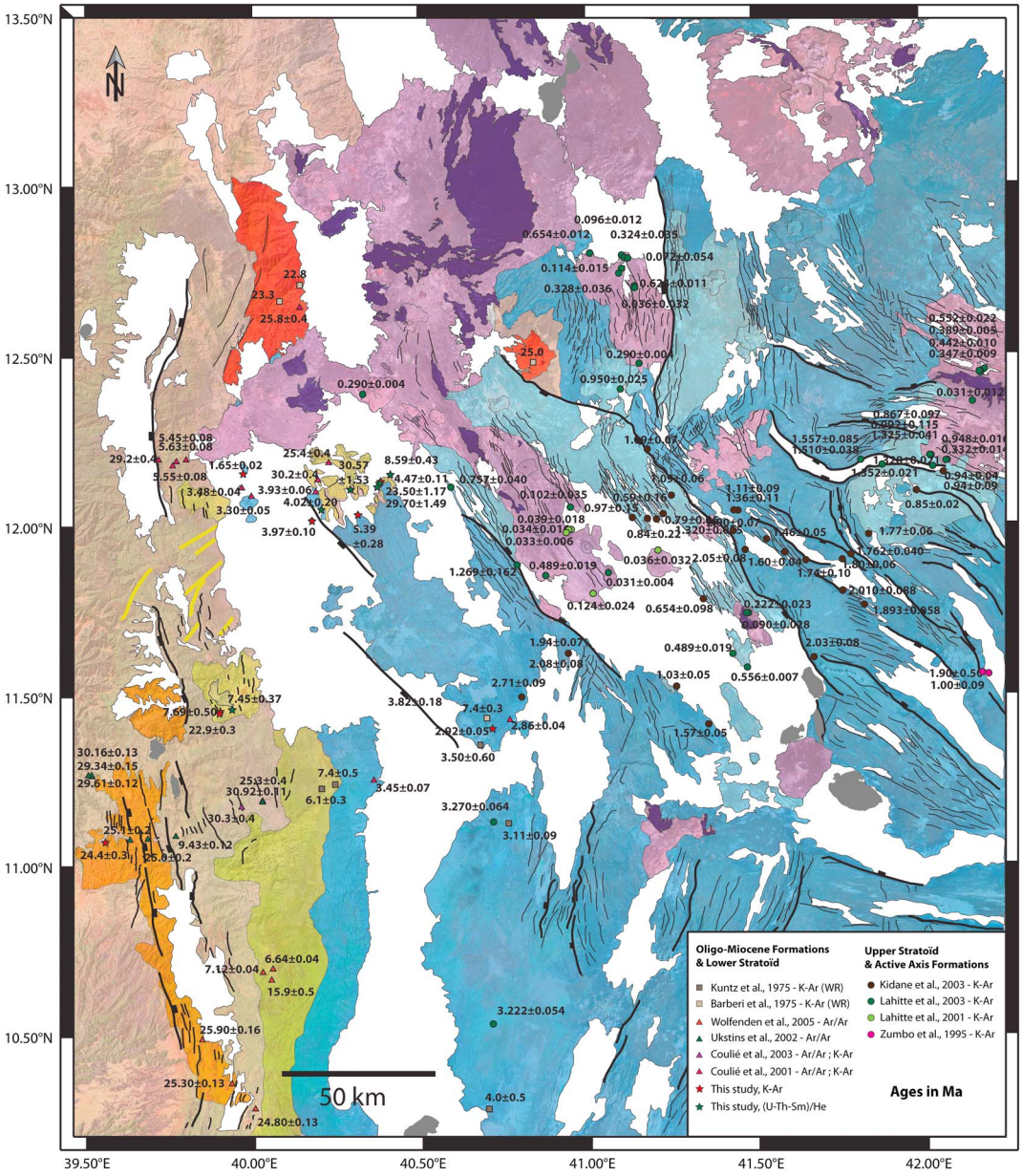

Figure 2. (continued)

the structural style of the future margin. We also discuss a number of problems concerning the distribution of volcanism in relation to rift segmentation. Finally, we compare Central Afar to other volcanic passive margins and discuss the process of SDR accretion and the significance of breakup in magma-rich settings.

2. Geological Setting

2.1. Present-Day Extension and Strain Accommodation

In this paper, Central Afar is defined as the broad zone of rifting that extends from the Ethiopian plateaus to the Gulf of Tadjoura (see Figures 1 and 2). We have named the topographic margin [e.g., *Wolfenden et al.*, 2005] the "Western Afar." Active volcanic segments mark the boundary between Nubia and Arabia (Figure 1), which separated during oblique rifting in the Red Sea and Gulf of Aden, which can be linked to the convergence of Arabia on Eurasia [e.g., *Bellahsen et al.*, 2003; *ArRajehi et al.*, 2010; *Leroy et al.*, 2012; *Faccenna et al.*, 2013]. GPS measurements constrain the NNE motion of Arabia with respect to Africa

[*McClusky et al*., 2010] and show that the strain shifts gradually south of 16°N from the Red Sea to the Afar and is totally accommodated in the Afar at 13°N. South of 13°N, the NW-SE trending rift structures of the Afar are truncated by roughly N-S trending faults of the Main Ethiopian Rift along the Tendaho Goba'ad Discontinuity (TGD) [*Harding et al*., 1990; *Hayward and Ebinger*, 1996, see Figure 1]. Plate reconstruction models predict a total extension factor of $ß > 3$ in Central and Southern Afar, assuming that the Danakil block (Figure 1) is a separate microplate [*Eagles et al*., 2002]. However, although the prerift structures are poorly documented, especially on the Danakil block, Jurassic limestones with tilts of 50–60° have been identified on the Danakil block [*Morton and Black*, 1975], suggesting high amounts of extension.

These high *ß* factors have been accommodated by the migration of strain from major border faults toward narrow strips of active deformation in the rift center [*Wolfenden et al*., 2005]. Later studies have suggested that such localization, from the rift border to narrow segments controlled by dyking, can be expected when the lithosphere becomes sufficiently weak [*Corti et al*., 2003]. In Central Afar, however, the strain is accommodated over a wide zone. *Kogan et al*. [2012] have shown that 90% of the present-day strain is accommodated over a broad strip of 175 km width. This strain pattern may be due to the presence of a weak mantle beneath the Afar [*Kogan et al*., 2012], to complex interactions between propagating rift systems in the area [*Pagli et al*., 2014] or to the presence of a faulting-dominated system [*Hammond et al*., 2011; *Keir et al*., 2013; *Pagli et al*., 2014].

2.2. Mantle Beneath Ethiopia

The mantle beneath Ethiopia is hotter than normal [*Benoit et al*., 2006; *Rooney et al*., 2012]. Seismic tomography studies show a broad low *P* wave velocity anomaly of 3% in the mantle beneath Ethiopia, which is rooted at a depth of ~500 km [*Li et al*., 2008]. This anomaly is thought to be the expression of the Afar plume, which was responsible for the extensive magmatism during the Oligocene in Ethiopia [*Baker et al*., 1996a, 1996b; *Marty et al*., 1996; *Hofmann et al*., 1997; *Pik et al*., 1999, 2006] and in Yemen [*Baker et al*., 1996a, 1996b], as well as for the dynamic topography that characterizes the Ethiopian, Somalian, and Yemeni plateaus [*Daradich et al*., 2003; *Pik et al*., 2008; *Stamps et al*., 2010]. This low velocity anomaly eventually connects with the Afar crust (at ~50 km depth, the limit of resolution) through narrow paths of channelization rather than a diffuse zone [*Hammond et al*., 2013]. This argues against the presence of a plume-head in the present day, and the magma ascent is therefore best explained by passive upwelling in response to lithospheric thinning [*Rychert et al*., 2012]. However, numerical modeling of the PT conditions necessary for the eruption of present-day basalts [*Ayalew and Gibson*, 2009; *Rooney et al*., 2012; *Ferguson et al*., 2013b] has shown that the Ethiopian mantle remains hot today, with an anomaly of +150°C, and that partial melting occurs at depth of ~80 km, even though the mantle beneath Ethiopia is one of the coolest of the world's continental and oceanic magmatic provinces [*Rooney et al*., 2012]. The Ethiopian mantle is also characterized by some of slowest seismic velocities on Earth. *P* wave velocities decrease from the classic mantle velocity (Vp) of 8.0 km/s, characteristic of the Main Ethiopian Rift (MER), and then level off to a slower velocity of 7.4 km/s, characteristic of anomalously hot mantle, beneath the Afar [*Bastow and Keir*, 2011]. *Kogan et al*. [2012] have shown that a substantial part of the lithospheric strength is borne by the lithospheric mantle beneath East Africa. Long period surface wave dispersion shows that this mantle thins beneath the Afar, from 100 km under the MER to less than 30 km [*Pasyanos et al*., 2009]. *Dugda et al*. [2007] argue for the possible absence of lithospheric mantle beneath the Afar on the basis of the absence of a lithospheric mantle lid in their observations.

2.3. Nature of the Crust, Magma Intrusions, and Underplating

Debate surrounding the nature of the crust, and whether it is of stretched and intruded continental nature (transitional crust) or is already oceanic crust, has been ongoing since the early work of *Berckhemer et al*. [1975]. Magnetic anomalies analogous to those of mid-oceanic ridges have previously been observed in Afar [*Bridges et al*., 2012], and ridge-like organization of the magmatic plumbing system, with on-axis and off-axis reservoirs, has been described in the Manda Hararo segment [*Medynski et al*., 2013]. Magma-assisted rifting has also been reported in the MER and Afar, where a shift occurs from fault-accommodated extension to dyke injection-accommodated extension at the active segments [*Grandin et al*., 2010; *Ebinger and Casey*, 2001; *Ebinger*, 2005]. *Casey et al*. [2006] argues for oceanic-type extension. However, recent trace element modeling of basalts from MER Pliocene-Quaternary lavas [*Rooney et al*., 2014a] and isotopic data from the Miocene shield on the plateau adjacent to the MER [*Rooney et al*., 2014b] suggest that the magma associated with rifting is derived from melting of phlogopite- and amphibolite-bearing mantle. Furthermore, they

suggest that the oldest magnetic stripes recorded in the lavas may in fact reflect intrusions into continental crust that strike parallel to the structures, and these should not be confused with oceanic-like intrusions.

Magma chambers are present at shallow depth beneath Alu Dallafilla volcano (at ~1 km depth) [*Pagli et al*., 2012] and Dallol volcano (at 1–2 km depth) in the Erta'Ale segment [*Nobile et al*., 2012]. A deeper magma reservoir, containing up to 13% melt fraction and 30 km wide and 35 km deep, has been identified beneath Manda Hararo [*Desissa et al*., 2013] (Figure 1). Vp/Vs ratios of 1.9 to 2.1 under the Manda Hararo/Sullu Adu zone (Figure 2) point toward the presence of partially molten mafic material in the crust [*Hammond et al*., 2011; *Dugda et al*., 2005]. Such high ratios imply the presence of fluids that are interpreted as partial melting stored in the crust [e.g., *Ahmed et al*., 2013; *Korostelev et al*., 2014]. A high velocity lower crustal layer (Vp = 7.2–7.4 km/s) has been identified documented beneath the shoulder of the MER but not beneath Afar. However, the lower crust velocity under the Afar increases from 7.0 to 7.4 beneath Erta'Ale [*Bastow and Keir*, 2011]. High velocities like these may be characteristic of mafic underplating [*Thybo and Artemieva*, 2013], but unfortunately, an insufficient number of across-strike seismic refraction profiles have been acquired to confirm the existence of a high velocity body under Afar or to constrain its spatial distribution. However, gravity modeling has shown that the crust must contain high density (3000 g/cm^3) mafic rocks in both the lower crust and the mantle in order to fit the observed prominent positive Bouguer anomalies [*Tessema and Antoine*, 2004].

2.4. Crustal Thinning

The thickness of the crust has been well constrained by receiver function computations and decreases from 35–40 km under the Ethiopian plateau to ~25 km under Central Afar and ~18–15 km under Northern Afar (Erta'Ale) [*Hammond et al*., 2011; *Reed et al*., 2014]. *Hammond et al*. [2011] identified sparse, 30 km thick slivers of crust under Afar (under Tendaho graben, Figures 1 and 2, for example), which they interpreted as remnants of less-stretched continental crust. However, more recently, *Reed et al*. [2014] applied a correction for the strong reflective phase of quaternary sediment infill in the Tendaho Graben and concluded that was actually only 20 to 18 km thick, giving an overall thinning factor (*ß*) of 2.0–2.2.

The thickness of the upper crust decreases from 22 to 25 km under the Ethiopian plateaus [*Makris and Ginzburg*, 1987; *Maguire et al*., 2006] to ~7 km beneath the Sullu Adu area (SW Manda Hararo, see Figure 2) (inverse modeling of receiver function data [*Hammond et al*., 2011]) and ~10 km under most of Central Afar (seismic refraction profiles in *Berckhemer et al*. [1975]). The lower crustal thickness seems to remain about the same beneath the plateaus and Central Afar, but thins abruptly under Erta'Ale. On the basis of modeling of dyking-accommodated extension, crustal thickness, and recent volcanism, *Bastow and Keir* [2011] argued that Erta'Ale is at a more advanced stage of rifting than Central Afar.

The equivalent elastic thickness of the lithosphere under Afar is ~6 km [*Ebinger and Hayward*, 1996; *Pérez-Gussinyé et al*., 2009]. This is thought to represent the upper crust as the strength of the mantle lithosphere beneath the rifted region is negligible [*Pérez-Gussinyé et al*., 2009], or has a low thickness (with a lithospheric lid at $\leq$50 km depth) [*Dugda et al*., 2007]. The seismogenic layer is ~7–9 km thick under Afar but 25–30 km thick under the plateaus [*Craig et al*., 2011]. These thicknesses are consistent with those of the early magnetotelluric study of *Berktold et al*. [1975], which used the electrical properties of rocks to set the depth of brittle/ductile transition at around ~6 km under Afar after determining a mean geothermal gradient of ~60°C/km. Under the plateaus, the long-term geothermal gradient is 35–38°C/km, as constrained by U-Th/He thermochronometry [*Pik et al*., 2003].

2.5. Stratigraphy and Volcano-Tectonic History

In this paper, the term syn-rift is used to describe rocks that were emplaced after the onset of extension in the area. Thus, even though the term is traditionally used to describe sequences that show syn-tectonic features (such as growth strata and extensional fans), it is used only in the temporal sense here.

Rifting in northeast Africa began during the late Eocene-early Oligocene in response to closure of the Tethyan Ocean [e.g., *Bellahsen et al*., 2003]. Rifting began at 26 Ma in the central and southern Red Sea [*Baker et al*., 1996a; *Ukstins et al*., 2002], after 29 Ma in the Afar [*Ukstins et al*., 2002; *Wolfenden et al*., 2005] and at around 34 Ma in the Gulf of Aden [*Leroy et al*., 2012, and references therein]. Oceanic spreading in the Gulf of Aden [*d'Acremont et al*., 2010; *Leroy et al*., 2012] began at around 18 Ma. Divergence between Somalia and Nubia began at around 11 Ma with the formation of a triple junction and opening of the MER [e.g., *Wolfenden et al*., 2004; *Corti*, 2009].

A regional continental flood basalt episode occurred in the Oligocene prior to the onset of any significant extension [*Pik et al*., 1998]. The bulk volume eruptions took place between 31 and 29 Ma [*Hofmann et al*., 1997; *Rochette et al*., 1998; *Coulié et al*., 2003]. The Trap Basalt formation overlies the older Jurassic sediments and Proterozoic basement. The Traps are also found in Ethiopia and Yemen [*Baker et al*., 1996a; *Ukstins et al*., 2002] and are a key feature of the Ethiopian plateaus. Trap Basalts are also found elsewhere on the Afar floor, notably in the Affara Dara massif (Figures 1 and 2) [*Barberi et al*., 1975; *Mohr*, 1978; *Varet*, 1978] and near the Western Escarpment [*Morton and Black*, 1975; *Ukstins et al*., 2002; *Wolfenden et al*., 2004, 2005]. The Traps are usually referred to as "prerift" structures as they predate extension.

During the Miocene, the cessation of flood basalt eruptions signaled a decrease in volcanic activity, at the same time as or shortly after the onset of extension in the region. Volcanic activity became mostly confined to large shield volcanoes on the plateaus [*Kieffer et al*., 2004]. In Djibouti, the Miocene lavas have been assigned to the historical Adolei, Mabla, and Dahla Formations [*Varet*, 1978; *Barberi et al*., 1975; *Audin et al*., 2004] (Figures 1 and 4a). In Central Afar, Miocene volcanics are sparser [*Ukstins et al*., 2002; *Wolfenden et al*., 2005; *Coulié*, 2001; *Le Gall*, 2014] (Figure 2). The Miocene record mainly consists of silicic series and no continuous record of volcanism has been mapped. Instead, in southern Afar, the volcanic units are separated by minor ($<10°$) angular unconformities [*Wolfenden et al*., 2004, 2005], indicating minor extension accommodated by faulting (see Figure 4). Farther south, where the MER overprints the Afar structures, the angular unconformities become more pronounced [*Wolfenden et al*., 2005].

A second pulse of flood basalt eruptions occurred during the Pliocene, beginning at around 4 Ma and with peak activity at around 2 Ma. With massive basaltic fissural eruptions that spanned the Afar floor, the Stratoïd Formation covers 70% of the rift surface. Above the Stratoïd Formation lie the Gulf Basalts, which were emplaced between ~1.1 and 0.6 Ma [*Kidane et al*., 2003]. Unlike the rest of the Stratoïd series, the Gulf Basalts erupted along silicic centers, most notably near the major southeast dipping fault scarps of the Tendaho and Tat'Ale grabens (Figures 1 and 2). The Gulf Basalts were first mapped and described on each side of the Gulf of Tadjoura, where the Gulf of Aden has been propagating into the Afar since around 1 Ma [*Manighetti et al*., 1998; *Audin et al*., 2004].

Present-day magmatism in the Afar is focused in discrete active segments. Extension is primarily accommodated by dyke injection in the crust [*Wright et al*., 2006; *Grandin et al*., 2010]. Morphologically, the structure of the segments resembles that of oceanic ridges [*Hayward and Ebinger*, 1996; *Medynski et al*., 2013, 2015], but the segments have formed within a transitional crust [*Hammond et al*., 2011]. They are therefore generally considered to be features indicative of the imminent breakup in Afar and are thought to represent the ocean-continent transition [*Medynski et al*., 2013], which is characterized by strong segmentation, rapid emplacement, and discrete spatial distribution.

2.6. Synthesis and Main Objective

The Oligocene Traps and recent/active magmatic centers and faults have been comprehensively mapped and studied in the Afar [e.g., *Hofmann et al*., 1997; *Rochette et al*., 1998; *Pik et al*., 1998, 1999; *Coulié et al*., 2003; *Grandin et al*., 2010; *Medynski et al*., 2013, 2015; and references therein]. The lithospheric structure has likewise received considerable attention [*Ritsema and Allen*, 2003; *Simmons et al*., 2007; *Bastow et al*., 2008; *Li et al*., 2008; *Pasyanos et al*., 2009; *Ritsema et al*., 2011; *Bastow and Keir*, 2011]. The Traps series have been linked to an early thermal mantle anomaly, and the present-day magmatic centers have mostly been interpreted in the context of Gulf of Aden and Red Sea interactions that have taken place over the past few million years. However, the Mio-Pliocene tectonics and magmatism have received relatively little attention. Consequently, key constraints, such as the amount of Cenozoic thinning/stretching and the ages and volumes of magma involved, are poorly quantified. As a result, the interactions between magmatism and tectonics could not be properly discussed so far, even though the Afar is a unique place to do so. In the following, we present our approach and the main results obtained on age constraints for magmatism and tectonic evolution.

3. Methods

3.1. Geochronology

In order to better constrain the age of the Mio-Pliocene volcanics and associated tectonic events, samples were collected between Central Afar and the Plateaus (Figure 2b). Two methods were used to determine

Table 1. K-Ar Analyses in This Study

Sample	Formation	Longitude	Latitude	K (wt %)	^{40}Ar* (%)	^{40}Ar* (10^{12} at/g)	Age (Ma)	± (Ma)
AF12-02	Stratoid ß	40.712	11.403	1.167	7.73	3.5246	2.89	0.06
					8.84	3.5870	2.94	0.05
						Mean	2.92	0.05
AF12-06	Transform volc. ß	39.970	12.157	1.269	28.73	2.1918	1.65	0.02
					27.68	2.1879	1.65	0.02
						Mean	1.65	0.02
AF12-11	Sullu Adu ß	40.382	12.133	0.126	5.87	0.5941	4.51	0.10
					4.08	0.5817	4.41	0.12
						Mean	4.47	0.11
AF13-82	Sullu Adu ß	40.280	12.034	0.121	2.69	0.6875	5.43	0.22
				0.086	1.27	0.4776	5.31	0.42
						Mean	5.39	0.28
AF13-90	Sullu Adu ß	40.174	12.026	0.366	4.68	1.5204	3.97	0.10
AF13-98	Chifra ß	39.897	11.459	0.089	3.43	0.7669	8.23	0.27
					3.77	0.6747	7.24	0.22
					3.17	0.7109	7.63	0.26
						Mean	7.69	0.50
AF13-99	Chifra ß	39.892	11.450	0.783	36.21	18.9568	23.0	0.3
					43.45	18.7734	22.8	0.3
						Mean	22.9	0.3
AF13-102	Dessie ß	39.520	11.077	0.565	50.53	14.4679	24.4	0.3
					47.29	14.5262	24.4	0.3
						Mean	24.4	0.3

the geochronology: (U-Th-Sm)/He dating of zircons and apatites from rhyolites and K-Ar dating of basalt and rhyolite samples. These methods date the instantaneous cooling of the volcanics and therefore their age of emplacement.

3.1.1. K-Ar

Samples were prepared and analyzed at the Geosciences Paris Sud laboratory, Université Paris-Sud (Orsay, France). The Cassignol-Gillot method of K-Ar dating has already been used to determine a large span of ages in the Afar [*Lahitte et al*., 2003a, 2003b; *Coulié et al*., 2003; *Kidane et al*., 2003] and our new K-Ar ages are consistent with previously obtained Ar/Ar ages, notably those of *Ukstins et al*. [2002] and *Coulié* [2001]. The K-Ar data of this study are presented in Table 1.

After careful examination of thin sections in order to eliminate the most altered samples, rock samples were sawed, crushed, and then sieved to obtain a homogenous fraction of typically 63–125 μm and 125–250 μm grain size.

Because lava phenocrysts can crystallize prior to eruption or be inherited from the magma chamber, they may contain excess Ar that leads to erroneously old ages. Phenocrysts should therefore be discarded from the sample. Magnetic separation and heavy liquids were used to separate out the phenocrysts from the basaltic groundmass and plagioclase (in basalt) or sanidine (in rhyolite) microcrysts used for dating. The end products of the separation process were basaltic groundmass of homogenous grain size and a density of 3.05 to 2.95 g/cm^3, plagioclase microcrysts with densities of 2.79 to 2.75 g/cm^3, and sanidine microcrysts with densities of 2.57 to 2.54 g/cm^3. K and Ar were measured on several aliquots of each sample according to the Cassignol-Gillot technique [*Gillot and Cornette*, 1986]. K was measured by flame absorption spectrophotometry. Argon-40 and ^{36}Ar concentrations were measured simultaneously by mass spectrometry. The amount of radiogenic ^{40}Ar* in the sample was then obtained after correcting for atmospheric contamination using the ^{40}Ar/^{36}Ar isotopic ratio of an air pipette. Each K and Ar measurement was performed at least twice in order to ensure a relative standard deviation of less than 1% for any given sample.

The uncertainty assigned to each individual age was then calculated using

$$\sigma_{age} = \sqrt{(\sigma_K)^2 + (\sigma_{Cal})^2 + (\sigma_{Ar^*})^2}, \quad (1)$$

where σ_{age} is the uncertainty in Ma, σ_K is the uncertainty in the K measurements (measurements were repeated on each aliquot until a relative standard deviation inferior to 1% was reached), σ_{Cal} is the uncertainty of the

Table 2. (U-Th-Sm)/He Analysis

Sample	Formation	Longitude	Latitude	Phase	^{4}He (10^{-9} mol/g)	^{238}U (ppm)	^{232}Th (ppm)	^{147}Sm (ppm)	He Age (Ma)	F_T	Corrected Age (Ma)	± (Ma)
AF12-21	Chifra Rhyolite	39.935	11.463	Zr	8.509	216.0	125.8	44.9	6.42	0.86	7.5	0.4
AF12-07	Finto Rhyolite	40.379	12.127	Zr	20.961	182.3	112.1	1834.8	18.43	0.81	22.7	1.1
				Ap	2.451	10.0	39.8	2501.4	20.22	0.83	24.3	1.2
										Mean	23.5	1.2
AF12-10	Traps	40.374	12.124	Zr	8.560	51.96	45.30	55.71	25.31	0.88	28.8	1.4
				Zr	8.522	49.84	43.04	59.99	26.31	0.86	30.6	1.5
										Mean	29.7	1.5
AF12-12	Finto Rhyolite	40.410	12.153	Zr	316.770	8245.51	5796.78	633.07	6.11	0.76	8.0	0.4
				Ap	14.933	387.29	270.23	951.87	6.13	0.67	9.2	0.5
										Mean	8.6	0.4
AF12-15	Sullu Adu Rhyolite	40.204	12.051	Zr	3.479	163.58	99.12	29.74	3.45	0.86	4.0	0.2
				Zr	2.360	113.37	65.39	16.64	3.40	0.84	4.0	0.2
										Mean	4.0	0.2
AF13-76	Traps	40.304	12.100	Zr	14.412	75.86	88.48	22.86	27.61	0.92	29.9	1.5
				Zr	10.236	57.25	65.78	22.35	26.07	0.90	28.9	1.4
				Zr	10.381	49.79	58.07	25.90	30.30	0.92	32.9	1.6
										Mean	30.6	1.5

mass spectrometer calibration and is inferior to 1%, and σ_{Ar*} is the uncertainty in the determination of the quantity of atmospheric ^{40}Ar in the sample. The latter was determined by comparing the ^{40}Ar/^{36}Ar ratio of the sample with the ^{40}Ar/^{36}Ar ratio of a standard air pipette under similar Ar pressure. Sample AF13-98 yielded more heterogeneous ages (see Table 1) than the other samples, and the uncertainty reported for this sample is therefore the standard deviation of the mean age.

3.1.2. (U-Th-Sm)/He

Samples were prepared at the Centre de Recherches Pétrographiques et Géochimiques and the Service d'Analyse des Roches et des Minéraux (Nancy, France), following the method described in *Pik et al.* [2003] and B. Tibari et al. (manuscript in preparation, 2015). The U-Th-Sm/He measurements are presented in Table 2. Rocks were crushed and sieved, and heavy minerals were then separated by densimetry. Aliquots of three to five zircon or apatite grains were prepared, and ^{4}He and U, Th, Sm concentrations were measured on each aliquot. Errors in the measured ages are equal to the reproducibility of standards (B. Tibari et al., manuscript in preparation, 2015) being 6% at a 1 sigma confidence interval. This level of precision is in agreement with those in the literature (see review in B. Tibari et al., manuscript in preparation, 2015). The uncertainty of the U-Th-Sm/He ages is higher than it is for K-Ar, the data can still be used to identify formations of Cenozoic age. For example, an uncertainty of 6% for an age of 30 Ma (the age of the Traps in this study) will yield an error of 1.8 Ma. The ages reported in Table 2 are therefore still consistent with those documented in the literature [i.e., *Ukstins et al.*, 2002; *Coulié et al.*, 2003]. Although the (U-Th-Sm)/He method may lack the precision required to discriminate between younger formations such as the Dahla and Stratoïd, the ages obtained can be compared with the more precise K-Ar ages of the basalts. A particular advantage of the (U-Th-Sm)/He method is that zircons and apatite are typically found in acid rocks, such as rhyolites, and it is therefore an ideal tool for mapping zones that contain a large abundance of acid magmatism.

3.2. Balancing Cross Sections: Polyphase Faulting and Tilted Blocks

The western part of Central Afar is composed of domino-style fault blocks bound by SW facing normal faults and tilted toward the center of the depression [*Zanettin and Justin-Visentin*, 1975]. These faults are numerous enough and have such throws that the resulting architecture is a strongly tectonized margin, with a smooth gradient in elevation from the escarpment toward the depression. The traditional method used to determine the extension factor (ß) in such environments is to calculate the amount of horizontal displacement created by the rotation of two adjacent blocks that were initially horizontal and contiguous [*Le Pichon and Sibuet*, 1981]:

$$\beta = \sin\theta / \sin(\theta - \phi), \tag{2}$$

where (θ) is the fault initiation angle and (ϕ) is the amount of rotation before fault lock-up. In "domino-models" such as this, a number of assumptions are made: (1) each fault generation initiates at the

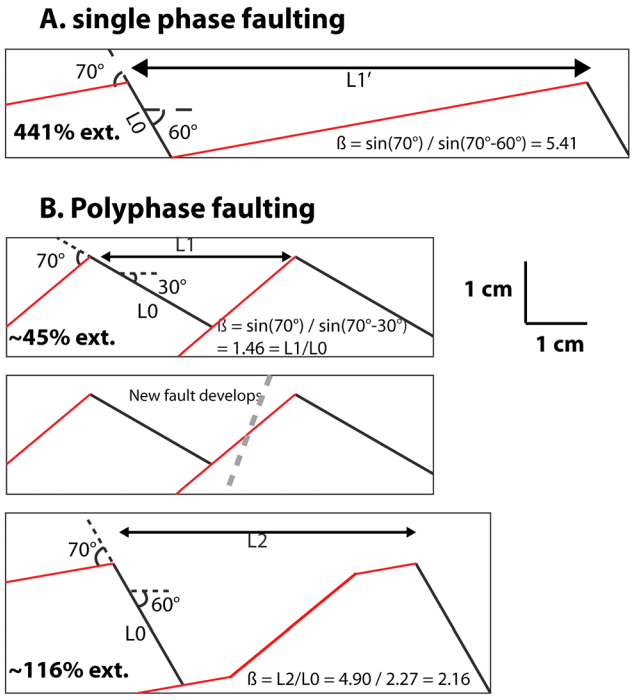

Figure 3. Surface stretching factor calculation for a single phase of faulting and for polyphase faulting bed dips of 60°. We assume a domino model with initially steep faults with dips of 70° and initial bed dips of 0°. Tilted blocks do not suffer any internal deformation, and thus, stress is only released by pure shear and extension is only accommodated on fault planes. Elevation differences between tilted blocks are neglected. The mathematical formula used to calculate *ß* is from *Le Pichon and Sibuet* [1981] (equation (2) in text). (a) Single faulting episode. Conditions are such that no second-generation faults initiate during extension. Blocks are tilted from 0° to 60° and extension is accommodated on the same fault plane. The corresponding accommodated extension is 441% (*ß* = 5.41). Note that after rotation the fault plane is nearly flat. (b) Polyphase faulting. A first-generation fault rotates the beds from 0° to 30°. At this point it is more favorable for a second-generation fault to develop so the fault consequently locks up. The second-generation fault rotates the strata from 30° to 60°. The first-generation fault planes are rotated to a nearly flat angle, whereas the second-generation fault plane dips to around 45°. The corresponding accommodated extension is 116% (*ß* = 2.16). The figure illustrates the impact of the number of fault generations on the surface stretching factor corresponding to observed strata dips: the greater the number of fault generations, the smaller the value of *ß*.

same dip, (2) blocks do not undergo any internal deformation, (3) the difference in elevation from one tilted block to another is small enough to be neglected at a local scale (e.g., along a ~25 km long transect), and (4) the rotation of each block is identical.

However, bedding dips as high as 60° have been encountered in the Afar [*Morton and Black*, 1975]. Mohr-Coulomb theory predicts fault initiation at 60–70° dip. From this simple perspective then, extreme bedding dips of 60° would correspond to subhorizontal fault planes and predict an infinite extension rate. Because flat or near-flat fault planes are never observed in Afar (Figure 3a), our favored model is therefore one of polyphase faulting [*Reston*, 2005], as illustrated in Figure 3b. The method has previously been used to resolve extension discrepancy and upper/lower plate paradox issues on the Iberia-Newfoundland sedimentary passive margins [*Reston*, 2005, 2007].

In the polyphase faulting model, a first generation of faults initiates at dips of 60–70° and then rotate until fault dips of ~35° are reached (Figure 3b). Once the first-generation faults have become inactive, a second generation of faults initiates to pursue extension. These second-generation faults then rotate and eventually lock-up, and the process is repeated (Figure 3b). The extension rate obtained after *n* generations of faulting is much lower than that obtained from a single fault generation model (Figure 3a). More extension is accommodated by near-flat fault planes than by a succession of steeply dipping faults.

4. Results

The Central Afar study zone encompasses the northern half of the map in Figure 2, extending from the Ethiopian plateaus, across the marginal graben, and through the depression (Figures 1 and 2). Toward the south, there is a shift from the NW-SE to NNW-SSE trending structures of the Red Sea, characteristic of Central Afar, to a NNE-SSW oriented grain that corresponds to the opening of the Main Ethiopian Rift through the Afar (Figure 1). We therefore focus our study on a cylindrical part of the margin, where all structures strike subparallel to the marginal graben and Manda Hararo active segment (Figure 2). The area was mapped using field observations, calibrated Landsat 7 composition with bands (7, 4, and 1), Universal Transverse Mercator (UTM) 37 N projection and satellite imagery (SPOT and Centre National d'Etudes Spatiales), and aerial photographs. In this section, we will refine the chronostratigraphical chart and structure of the Central Afar rift by focusing on two key localities, Arabati and Sullu Adu (Figure 2), which correspond to a proximal zone (east of the marginal graben) and a more distal zone in the depression, (west of the Manda Hararo active segment),

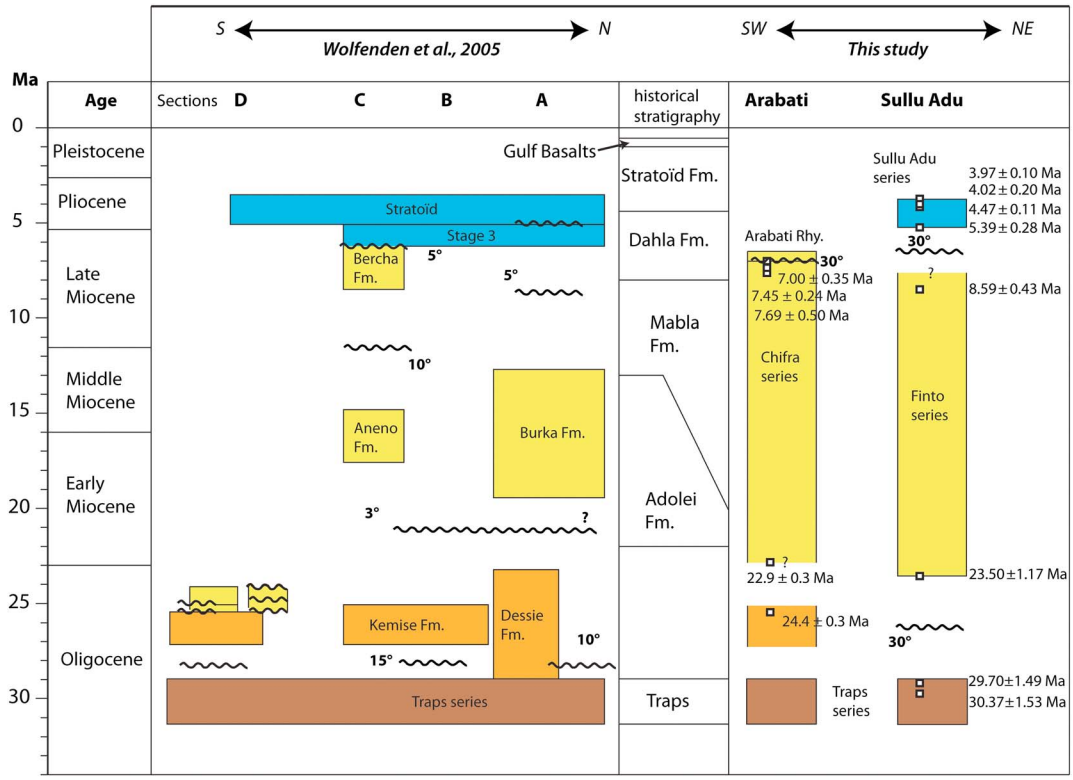

Figure 4. Volcano-stratigraphic chart of Central Afar and Djibouti. (left) Compilation from *Wolfenden et al.* [2005] of local volcano-stratigraphic records mapped along four transects (A, B, C, and D) that show the along-strike N-S evolution of Western Afar. The transects document the transition from N-S trending structures representative of the MER (profiles D and C), to NW-SE trending structures representative of the Red Sea tectonic grain (profiles B and A). (right) Spatio-temporal evolution of volcano-stratigraphy along a SW-NE cross section (see Figure 2a) based on new age data and field observations of this study. Wavy lines represent angular unconformities. Values in degrees (°) are the difference in dip between the two discordant units. Straight contacts represent conform volcanic units. Question marks indicate inferred contacts between units (contact was not observed) (see text for more information). The (U-Th-Sm)/He and K-Ar age data of this study are shown in the right panel (in Ma, 1 sigma uncertainties; see Tables 1 and 2). For comparison, the central column shows historical formations mapped mainly in Djibouti and then extended to the rest of Afar [after *Varet*, 1978, and references therein].

respectively. We first present new field data and radiometric ages in an attempt to unravel the tectono-magmatic evolution. We then synthesize the results along a balanced composite cross section in order to link surficial and deep structures.

4.1. Volcano-Stratigraphy of Central Afar

A local stratigraphic chart for the Arabati and Sullu Adu areas is presented in Figures 4a and 4b. The ages obtained from K-Ar and U-Th-Sm/He techniques are presented in Tables 1 and 2, respectively. The results are summarized in Figure 4, which shows the south-north distribution of ages along the western part of Central Afar, based on the stratigraphic charts of profiles A, B, C, and D in *Wolfenden et al.* [2005] (see Figure 2). This is compared to a west-east variation that reflects the time span of lava formations along our study profile (Figure 2). We were able to distinguish four units, which are separated by angular unconformities.

4.1.1. Oligocene Flood Basalts

The Traps formation is recognizable in the Sullu Adu area by the U-Th-Sm/He ages of 29.7 ± 1.5 and 30.6 ± 1.5 Ma of strongly tilted rhyolites (AF12-10 and AF13-76; Figure 4b). These ages are in agreement with the age of *Coulié* [2001] of 30.2 ± 0.4 Ma obtained at the northernmost tip of the Sullu Adu area (Figure 2b). Although we did not date any samples of the Traps in the Arabati area, they are most likely present below the Miocene volcanics [*Ukstins et al.*, 2002; *Wolfenden et al.*, 2005] (see below). We can correlate the Trap formation in Sullu Adu to the Trap Basalts observed elsewhere in Western Afar and on the plateaus.

4.1.2. Miocene Basalts and Rhyolites

The marginal graben basalts near Dessie yield a K-Ar age of 24.40 ± 0.35 Ma (sample AF13-102; Figure 2b). We did not observe any unconformity between this formation and the underlying Traps. Given the age range and similar rock types, we correlate this formation to other local marginal graben-related volcanics (Dessie and Kemise Formations) [*Wolfenden et al*., 2005] (Figures 1, 2, and 4). These upper Oligocene formations appear to be restricted to the present-day marginal grabens and are not found in Arabati or Sullu Adu (Figure 2). This may suggest that the eruptions at 25 Ma were localized in a protomarginal graben.

In contrast, early to late Miocene volcanic formations are found in both the Arabati and Sullu Adu zones. In Arabati, the age of Chifra series is bracketed between 22.9 ± 0.3 Ma (AF13-99, K-Ar) and two ages of 7.69 ± 0.50 (AF13-98, K-Ar) and 7.5 ± 0.4 Ma (AF12-21, (U-Th-Sm)/He, Figure 4b). However, as it was not possible to observe the contact between the tilted Arabati series and the Traps, the lowermost part of the series may well be older than this. A series as old as 25 Ma, i.e., as old as the basalts of the marginal graben, might therefore exist.

In Sullu Adu, the base of the Finto series has an age of 23.5 ± 1.2 Ma (AF12-07, (U-Th-Sm)/He, Figure 8). The sample was taken from an ignimbrite layer lying conformably above a layer of green tuff. This tuff is a commonly observed stratigraphic marker throughout the area and lies unconformably above rhyolites and basalts of the Traps formation (Figure 9). The top of the Finto series has an age of 8.6 ± 0.4 Ma (AF12-12, (U-Th-Sm)/He), but the upper limit for this series may be younger. Given the age correspondences between the two study areas, we correlate the Chifra and Finto series and argue that they erupted simultaneously.

Little to no extension appears to have occurred during the emplacement of these series as no internal unconformities were observed. Moreover, no intermediate ages (i.e., between 22 and 9 Ma) were determined within the formation. This suggests that the volcanic activity was either sparse, consisting of only two significant events, or was continuous but with relatively low volumes. This Miocene formation can be correlated to other formations found toward the south, namely, the Burka, Aneno, and Bercha Formations [*Wolfenden et al*., 2005] (Figure 4). In these locations, the Miocene series contain several unconformities: in profile A (Figure 4), the Burka Formation is apparently continuous [*Wolfenden et al*., 2005], whereas in the MER profiles B and C, a 10° discontinuity separates the ~16 Ma Aneno Formation from the ~7 Ma Bercha Formation [*Wolfenden et al*., 2005]. In profile D this corresponds to a MER-type orientation, the early Miocene record being truncated by three angular unconformities [*Wolfenden et al*., 2005].

4.1.3. Pliocene Flood Basalts

The flat-lying Arabati and Sullu Adu series (Figure 8) occupy the top of the volcanic record in our study areas. We dated the Sullu Adu flat-lying basaltic formation at several places along the NE-SW Sullu Adu transect (Figure 8) and obtained ages of 5.39 ± 0.28 (AF13-82, K-Ar), 4.47 ± 0.11 (AF12-11, K-Ar), 4.0 ± 0.2 (AF12-15, (U-Th-Sm)/He), and 3.97 ± 0.10 Ma (AF13-90, K-Ar). *Coulié* [2001] determined a similar age of 3.93 ± 0.06 Ma for a rhyolite located farther north. These results are consistent with our age of 2.92 ± 0.05 Ma (AF12-02, K-Ar) obtained south of Sullu Adu, near the Mille River (see Figure 2b). Given these ages, we correlate the Pliocene flood basalts with the lower Stratoïd Formations found elsewhere in Afar.

One sample from the Awra plain yielded an age of 1.65 ± 0.02 Ma (AF12-06, K-Ar, Figure 2b). This upper Stratoïd age argues in favor of late uplift of the Sullu Adu area. Thus, after emplacement of the Stratoïd Formation, the Sullu Adu area was uplifted while the Awra basin subsided and was filled with volcanic products until at least ~1.6 Ma.

Unfortunately, we were unable to find any suitable material with which to date the flat-lying Arabati rhyolites (Figure 8). However, these lie flat over the tilted Miocene Chifra series in the same way as the Sullu Adu basalts lie over the tilted Finto Miocene series. We therefore correlate these two volcanic units and can infer that the Arabati rhyolites most likely have an age of between 8 and 4 Ma. Because of the occurrence of 6 Ma old acidic rocks north of our profile (Figure 2b), we can correlate the Arabati rhyolites with Stage 3 of *Wolfenden et al*. [2005] (see Figure 4).

4.2. Structural Features of Central Afar

4.2.1. Arabati (Flexure Area)

The Arabati area (Figures 2, 5, and 6a–6d) is part of the flexure zone, which has been preserved from significant erosion. Farther north, erosion has been more intensive, and the only markers of past volcanism that remain are feeder dykes that intruded the Traps (Figure 2). Topographically, the Arabati area remains high,

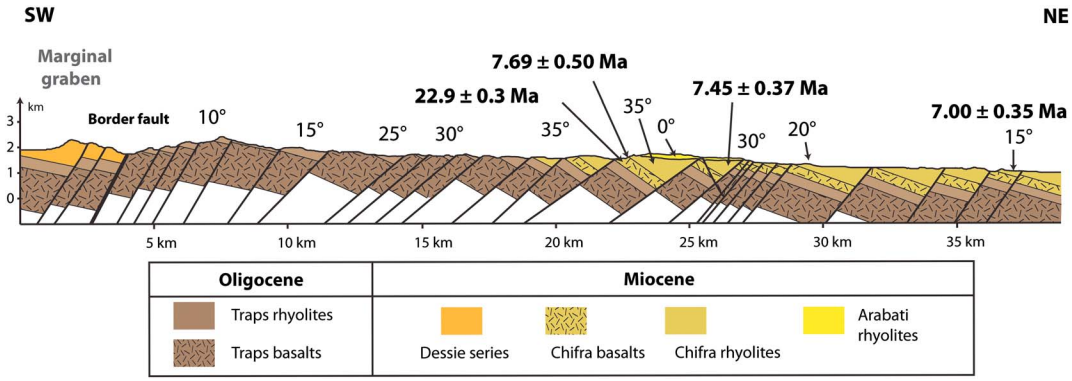

Figure 5. Cross section from the marginal graben through the Arabati study zone (see Figure 2a). The "Western side" is the zone of Oligocene outcrops, where Trap basalts and rhyolites are found, progressively flexured toward the NE. The "Eastern side" represents the Arabati zone, where outcropping Miocene Chifra and Arabati series lie unconformably over the Traps. Bedding dips and ages are also shown.

with an elevation that decreases slightly, from ~2000 to ~1500 m, in a northeastward direction (Figure 5). The area consists of a tight network of tilted blocks with observed faults that strike between 150°N and N-S and dip WSW (Figures 5 and 6c). The blocks tilt toward the rift center (northeastward) and the main faults are typically spaced 1 to 5 km apart (Figures 5, 6c, and 6d). These observations are consistent with the description given in *Zanettin and Justin-Visentin* [1975]. The easternmost tilted blocks of Arabati are buried beneath the present-day sedimentary infill of the Awra Plain around the town of Chifra, at an elevation of ~900 m (Figure 6). The area can be divided into two parts: the western side, which contains the Oligocene Traps (Figure 5), and the eastern side, where the Miocene lavas outcrop (Figures 5 and 6).

In the western part of the flexure area, the Traps series lies subhorizontally in the footwall of the west dipping marginal graben border fault (Figure 5). The dip then increases progressively from 10°NE to 40°NE at Arabati (at 22 km on the cross section in Figure 5), forming a flexure. The Traps are then buried under Miocene volcanics in the eastern part of the flexure area (Figure 5). In our balancing calculations, we assume that the Traps series is 2 km thick, as is commonly reported in the literature [e.g., *Hofmann et al*., 1997].

In the eastern flexure area, the Chifra series consists of a series of basalts, which lie below interbedded rhyolites and tuffs capped by a massive white rhyolitic unit. The dip of the Chifra series decreases from 35°NE at Arabati to 10–15°NE at the northeasternmost tip of the study area (Figures 5–7). The angular relationships between the Chifra series and the Traps series are unclear as no contacts were observed. However, given the smooth variation in dip between the traps to the west and the tilted Chifra series to the east, the existence of an abrupt unconformity of 30° between the two is unlikely. This suggests that either little extension occurred between the emplacements of the Traps series and Chifra series, or that tilting of the Traps to the west occurred synchronously after emplacement of the Chifra series. It is interesting to note that no thickness variations, unconformities or growth strata are observed within the Miocene series, indicating that significant deformation most likely took place after the whole unit had been emplaced.

The Arabati flat-lying rhyolites series is also observed in the eastern part of the flexure area, lying horizontally and unconformably above the 30°-dipping Arabati series (Figures 5, 6a, 6b, and 7). The Arabati flat-lying rhyolites are 100 m thick at most, and have been affected by a few NE dipping normal faults (Figures 6a and 6b). The total stretching factor accommodated by the Arabati flexure is $\beta = 1.30$ (obtained by measuring the initial length of the base of the traps).

4.2.2. Sullu Adu (Area of Highly Tilted Blocks)

We remapped the area as far as the northernmost tip of the Sullu Adu range, a prominent positive topographic anomaly in the Awra basin (Figures 2 and 8). In previous mapping studies, the area was reported to be mostly covered by the Dahla Formation [*Varet*, 1978] and was interpreted to be a protorift axis corresponding to an episode of localization of deformation at 8 Ma [*Audin et al*., 2004; *Hammond et al*., 2011]. In our mapping, however, we identified three distinct formations separated by angular unconformities (Figures 4b, 8, and 9a–9c). The youngest formation is a thin (50 m) undeformed layer of basalt that caps the tilted blocks. This flat-lying Sullu Adu basalt is the main feature observed in the Sullu Adu range (Figures 8 and 9b).

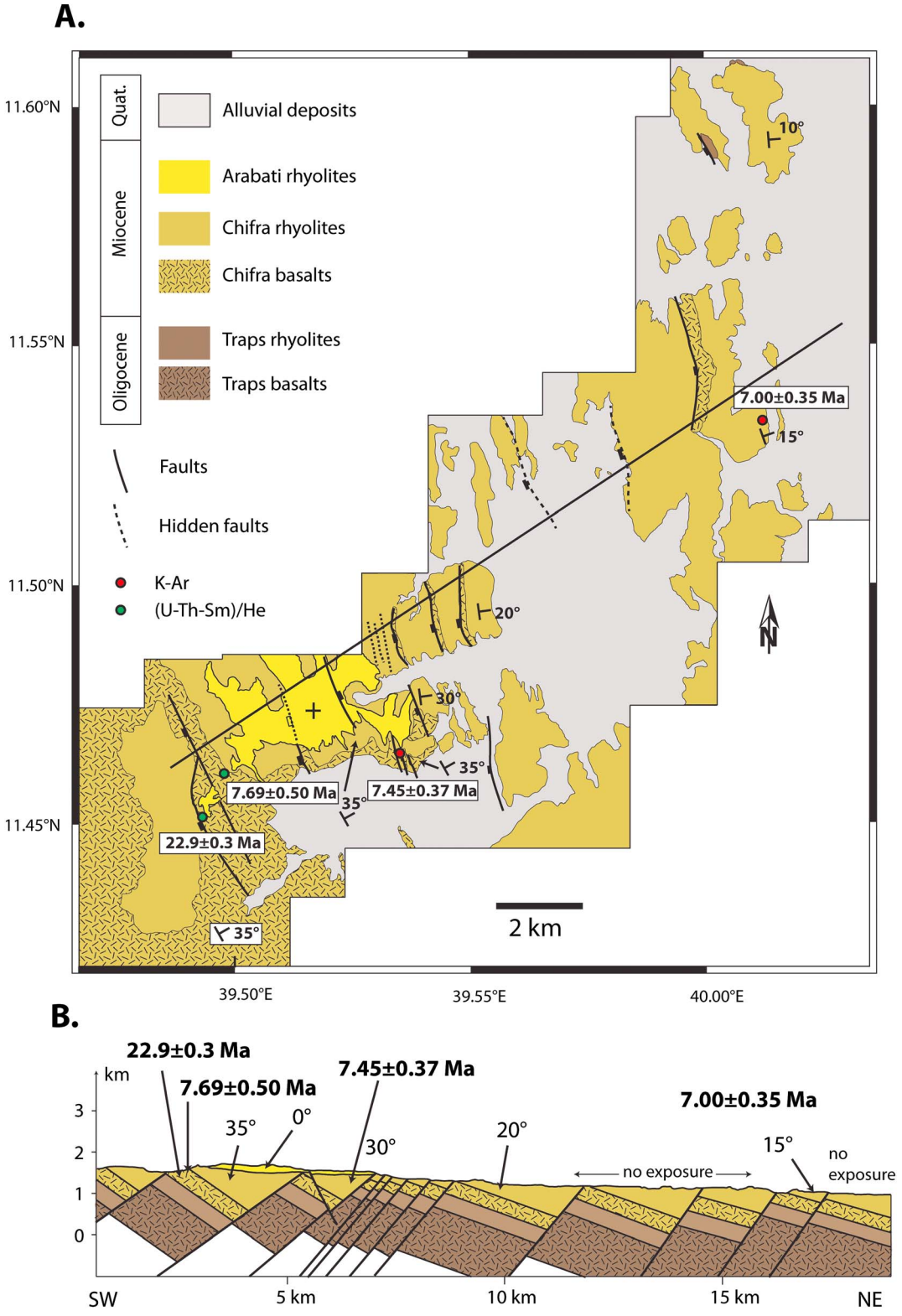

Figure 6. (a) Geological map of the Arabati area, WGS84, UTM 37 N, inset in Figure 2a. Maps were constructed using SPOT and Landsat (7, 4, and 1) images calibrated with field observations. (b) Cross section of the Arabati area, (Eastern Side in Figure 5). Mapped faults are projected onto the cross section. Emphasis is put on the angular relationship between the tilted Chifra series and the flat-lying Arabati series. The relationship with the underlying traps is unclear. Two faults were hypothesized (dotted lines or "hidden faults") based on the observation of topographic ridges on the satellite images.

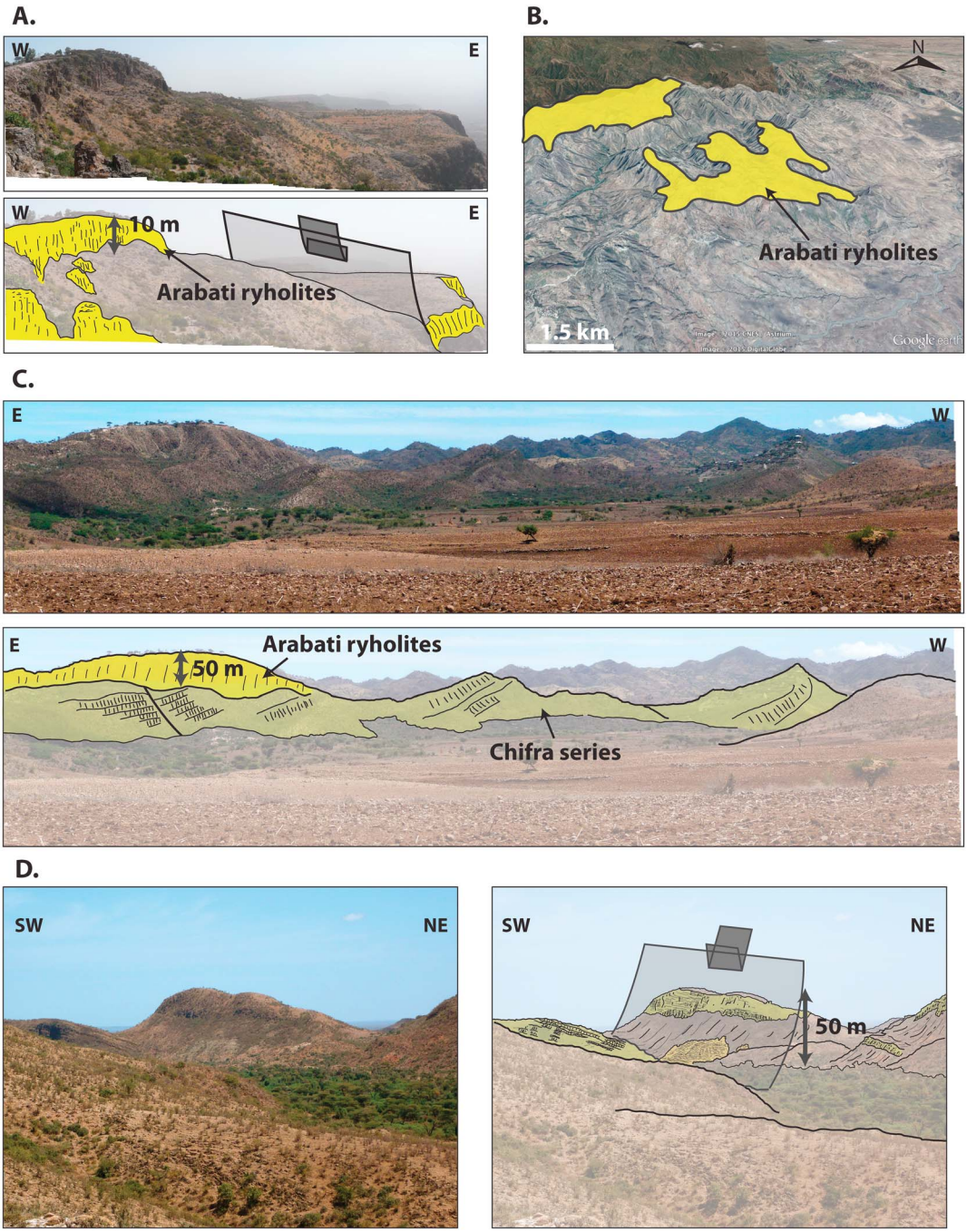

Figure 7. Field photographs of the Arabati area. (a) Flat-lying rhyolites of the Arabati series, represented in bright yellow. The Arabati rhyolites form a flat plateau (see Figure 6) affected by a single NE dipping normal fault. (b) Google Earth view of the Arabati plateau (outlined in bright yellow) over the Miocene tilted blocks (uncolored). (c) E-W view of the 50 m thick Arabati rhyolites (bright yellow) lying unconformably over the tilted Chifra series (pale yellow). The tilted blocks of the Chifra series dip E-NE. (d) Typical tilted block of the Chifra series. These tilted blocks have the fault plane preserved, with a throw of at least 50 m. The upper part of the series is composed of rhyolites (pale yellow) and the basal part is composed of basalts (pale yellow/orange), which outcrop in the footwall of the fault.

The tilted blocks are composed of the Traps and Miocene Sullu Adu series. These dip to the NE and are bound by west to SW dipping normal faults (Figures 8 and 9a–9c). The ~1 km spacing of the tilted blocks is tighter than it is in Arabati (Figure 8). This most likely indicates that the crust has been thinned more here than it has in Arabati. This is consistent with the lower bulk elevation (~600 m above sea level) compared to Arabati,

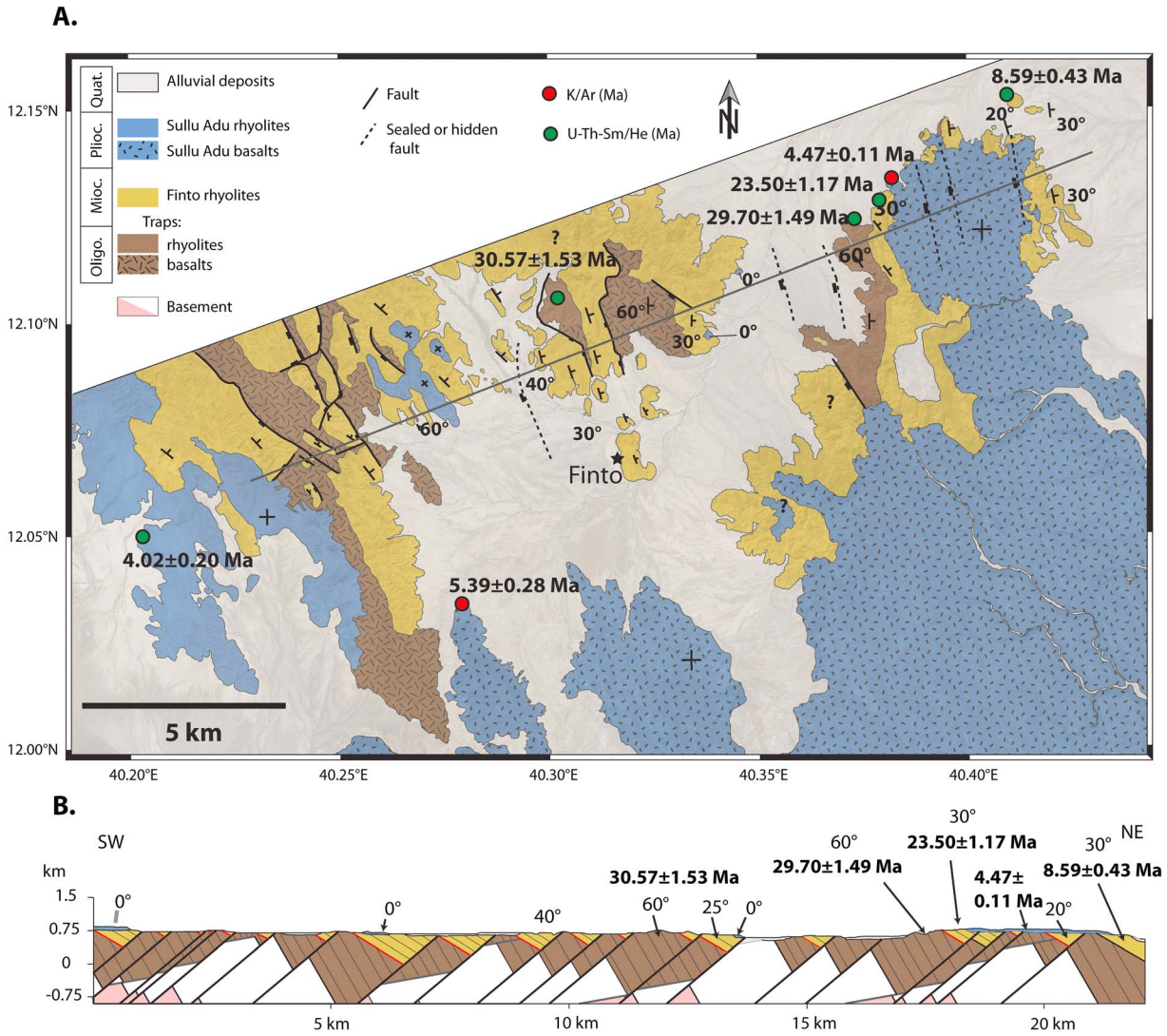

Figure 8. (a) Geological map of the Sullu Adu area, WGS84, UTM 37 N, inset in Figure 2a. Map was constructed using SPOT and Landsat (7, 4, and 1) images calibrated with field observations. A SPOT image is shown in transparency to illustrate the extent of the drainage system. The most prominent feature on the map is the flat-lying Sullu Adu basalts (blue and hatched). The rhyolitic equivalent of the Sullu Adu basalts, the Sullu Adu rhyolites (of similar age and also flat lying), is present on the western side of the map. (b) Cross section of the Sullu Adu area. Mapped faults are projected onto the cross section. The reconstruction assumes that (1) all mapped faults are second-generation faults (i.e., steep-faulted contacts between the Traps and the Miocene Finto series) because no flat faults were observed, (2) the throw of first-generation faults is never higher than 1.5 km so that the basement is never exposed, and (3) the Sullu Adu basalts and rhyolites are strictly unaffected by any faults (see text for more information).

and the Traps in this region do appear to have undergone intense deformation as they are found dipping at 60°E-NE at three localities (Figures 8 and 9a–9c). This dip direction appears to be constant over the whole area and is a key feature of the Sullu Adu area.

The Miocene series (in yellow in Figures 8 and 9) are tilted 30° ± 5° above the traps, indicating that an episode of extension took place between the emplacement of the Traps at 30 Ma and emplacement of the Miocene series at ~27–23 Ma. This age is consistent with the period of marginal graben extension and volcanism. This suggests that a period of distributed stretching, from the marginal graben area to the present-day Central Afar area, occurred at around 25 Ma.

It is noteworthy that the bedding dips observed in the Miocene series are similar to the flexure of the Arabati area. This suggests that a second episode of stretching, which occurred after 7 Ma, was also distributed spatially and affected both areas in a comparable way. This second extensional episode ended with the emplacement of the flat-lying Sullu Adu series of the Stratoïd Formation.

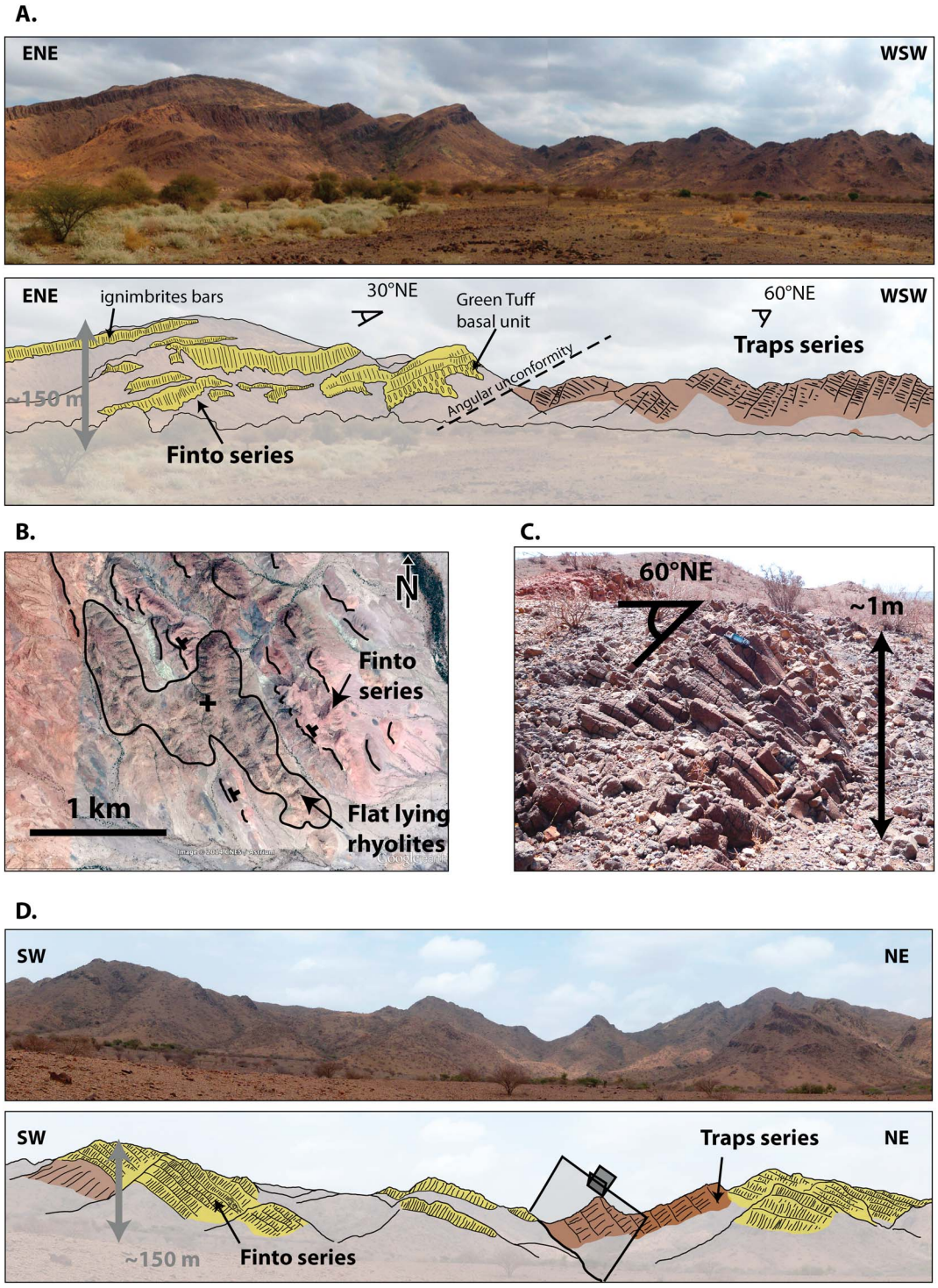

Figure 9. (a) Angular unconformity between the Traps (in brown) and the Finto series (bright yellow). (b) Google Earth image of the Sullu Adu flat-lying rhyolites. Although not dated, we correlate the rhyolites of limited extent (kilometer scale) to the acidic formation in the west of the map in Figure 8 (because the rhyolites unconformably overlie the tilted blocks of the Finto series and are also flat lying). These structures are present throughout the studied area, suggesting that the eruption of the Sullu Adu basalts and rhyolites was widespread. (c) Basaltic columns of the Trap series on which the dip of the strata (60°NE) can be measured. The columns form perpendicular to the surface of the flow, and thus, flat-lying flows display vertical columns. Handheld GPS device is shown for scale on the top of the columns. (d) Two tilted blocks separated by a SW dipping normal fault, a typical tectonic pattern in the Sullu Adu area. Finto series in bright yellow, Trap Basalts in brown.

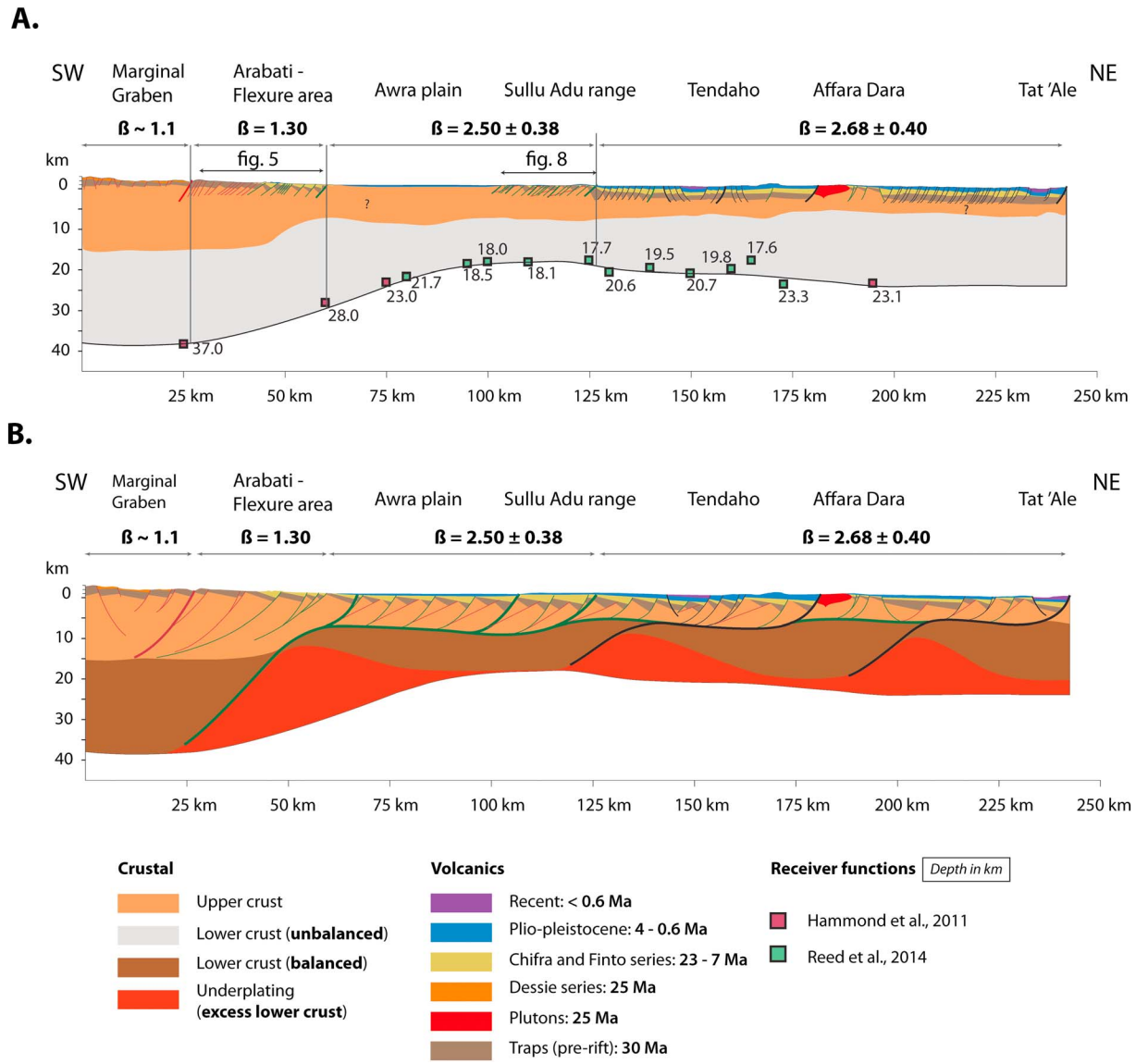

Figure 10. Composite cross section of Central Afar constructed from field observations at Arabati and Sullu Adu and data from the literature (see text). (a) Composite cross section with no vertical exaggeration. Surface stretching factors are given for each zone. Position of the upper/lower crust boundary is based on literature. The surface (area?) of the lower crust is too large in respect to the upper crust and the section is not balanced, implying an excess of lower crust. (b) Reinterpreted cross section of Central Afar that takes into accounts underplating in the lower crust. Polyphase faulting is represented as the tectonic style of the upper crust. Second-generation faults (in green) crosscut the older first-generation faults (red) and are rooted on a midcrustal shear zone that links distributed extension at the surface (upper crust) to localized deformation in the lower crust. The underplating is stored where crustal thinning has left in a gap in the lower crust. The process is then repeated as third-generation faults (black), absent in the Arabati and Sullu Adu areas, connect to younger shear zone beneath the Tendaho/Tat'Ale area. The three underplated bodies in this cross section are required in order to balance the lower crust with respect to the upper crust.

One problem encountered when attempting to balance the Sullu Adu cross section (Figure 8) was the 60° dip of the prerift Oligocene traps (Figures 9a and 9c). We followed the method described in section 3.2 and assumed that the faulting was polyphase. In our reconstruction, the first generation of faults displaced the Traps series at around 23–25 Ma. A second generation of faults then affected the Finto series between 7 Ma and the emplacement of the Stratoïd series at 4 Ma. These later faults also affected the earlier tilted blocks, resulting in rotation of the Traps to 60°. Our main limitation was that we were only able to map the second-generation faults, i.e., the steep contacts between the traps and the younger Miocene rocks. In most cases, the first-generation faults (i.e., those that only affected the Traps prior to emplacement of the Finto

Table 3. Stretching Factors

Domain	Final Length (%)	ß (70°)	ß (65°)	ß (61°)	Mean
M. Graben	11	~1.05	~1.05	~1.05	1.05
Arabati[a]	13	1.3	1.3	1.3	1.3
Sullu Adu	28	2.13	2.50	2.88	2.0 ± 0.4
Tendaho/Tat'Ale	48	2.28	2.68	3.08	2.7 ± 0.4
$ß_{WEIGHTED}$	100	1.81	2.00	2.13	2.0 ± 0.2[b]
	100				2.2[c]

[a]Measured on initial length of Traps for the western side and initial length of Chifra rhyolites on the eastern side, see text.
[b]Obtained after the calculation of the weighted mean of surface ß.
[c]Obtained after the balancing of the total area of (upper crust + lower crust) − (underplating).

series) were not observed; we did not observe any flat fault planes and, moreover, anomalous contacts within the Traps series are difficult to map. The resulting geometry shows that some of the second-generation faults have accommodated more displacement than others (Figure 8). This is consistent with the large variation in the orientation of the mapped structures. From west to east, the strike of the tilted blocks changes from ~N160° to almost N-S in the vicinity of Finto and then back to N160°.

4.3. Composite Balanced Cross Section

In this section, we present a balanced cross section of Central Afar (see Figures 10 and 2a for location), which we built from the sections described above (Arabati and Sullu areas; Figures 5, 6, and 8). We then compare our calculated crustal stretching to the crustal thinning observed in geophysics. First, we present the surface extension factor for each zone (Arabati, Sullu Adu, and Tendaho/Tat'Ale). These were extrapolated into tectonic "domains" on the cross section (Table 3 and Figure 10a). The upper crust below each domain was then balanced in order to check for consistency in the calculations assuming the conservation of area. The upper-lower crust boundary was reconstructed using the literature described in section 2.4. Next, we balance the lower crust beneath the Awra/Sullu Adu and Tendaho domains and identify any excess lower crust beneath the cross section, which we interpret to be syn-rift magmatic underplating, i.e., post-Traps magmatism (Figure 10b). Finally, we propose the existence of a low-angle midcrustal shear zone, which links the distributed stretching at the surface with the localized thinning in the lower crust. Shear zones such as this would also influence the spatial distribution of the excess lower crust (Figure 10b).

4.3.1. Amount of Extension at the Surface

The first step was to estimate the surface extension factors for the different domains (Table 3 and Figure 10a). We subdivided the cross section into several domains (Figure 10a). The length of these domains is expressed as relative length with respect to the total cross section length (for example, the length of the Arabati domain is 13% of the total cross section length). The marginal graben area experienced extension of about $ß = 1.05$. The Arabati area has a local extension rate of $ß_{Arabati} = 1.30$ (see 4.2, Figure 10 and Table 3). In Sullu Adu, ß depends on the initial dip of the faulting (Table 3), which was between 70° and 61° (Table 3). Because this variation is sizeable and because the initial dip of the faults was difficult to constrain, we chose to express the local ß for Sullu Adu with an error bar equivalent to the mean value of ß (2.50 ± 0.38; Table 3). For the Awra plain (Figure 2), we used the same ß as for Sullu Adu, which means that the combined length of Sullu Adu + Awra is 28% of the total length (Table 3 and Figure 10a). A ß value of 2.50 ± 0.38 was eventually reached between 7 (the end of Finto series emplacement) and 4 Ma (the onset of Stratoïd series emplacement). The ß for Tendaho area is the same as for Sullu Adu, multiplied by 1.07, which is the mean value of ß accommodated by the post-Stratoïd structures [*Acocella et al*., 2008]. Thus, we obtained a ß value of 2.68 ± 0.40 for the area from Tendaho to Tat'Ale (Table 3 and Figure 10a). It was then possible to check whether the extension accommodated by faulting at the surface was equivalent to the thinning of the upper crust beneath each domain. For this, we assumed the upper-lower crust boundary to be at 15 km depth beneath Arabati and 7 km depth between Awra and Tat'Ale [*Berktold et al*., 1975; *Pérez-Gussinyé et al*., 2009; *Craig et al*., 2011; *Hammond et al*., 2011]. The upper crust beneath Awra-Sullu Adu (~590 km^2) (Figure 10a), when balanced to a 15 km thick prerift stage, displays a stretching factor of ~2.7, which is consistent with the calculated value of 2.5 ± 0.38 (Table 3). The upper crust beneath Tendaho-Tat'Ale (~730 km^2) displays a stretching factor of ~3.0, also consistent within error with the value of 2.68 ± 0.40. This means that, in the present study, the amount of extension accommodated by faulting is a good proxy for the amount of

upper crustal thinning. Because we defined the base of the upper crust as the boundary between brittle and ductile behavior, the depth variation of this boundary should be temperature dependent as well as extension dependent. However, as our results show good agreement between surface stretching and upper crustal thinning, the depth variation over time that results from differences in heat flux can be neglected. Moreover, the effects of magma advection in the upper crust are probably also extremely local and can therefore also be neglected at this spatial scale. Thus, extension exerts the primary control on the thickness of the upper crust.

A final verification consisted of calculating the weighted mean of the sum of the initial length of the tectonic domains, weighted by the *ß* of each tectonic domain. This gives a virtual $ß_{WEIGHTED}$ of 1.98 ± 0.16. Of note, balancing the whole upper crust surface (~2440 km^2) back to an initial thickness of 15 km gives a *ß* of ~2.16, which is in good agreement with the model. Note however that here, *ß* describes the thinning of the entire cross section and thus depends on how much undeformed length is included in the balance calculations. Thus, the "weighted mean *ß*" value of ~2 is representative of the cross section alone and confirms only that our surface estimations are correct. However, the "real" *ß* value of $\sim 2.7 \pm 0.4$ corresponds to the extension experienced in the most stretched part of Central Afar, i.e., from Sullu Adu to Tat'Ale (Figure 2), and is comparable to other values of *ß* reported in the literature, notably those obtained in plate kinematics reconstructions [*Eagles et al*., 2002; *Redfield et al*., 2003]. Our stretching factor is however higher than the *ß* value of ~2.0 predicted by receiver functions analysis [*Hammond et al*., 2011].

4.3.2. Total Thinning Factor and Excess Lower Crust

The depth of the Moho was determined by receiver functions analysis [*Hammond et al*., 2011; *Reed et al*., 2014]. We inferred the depth of the upper/lower crust boundary by combining observations from the literature [*Berktold et al*., 1975; *Pérez-Gussinyé et al*., 2009; *Craig et al*., 2011; *Hammond et al*., 2011]. The Moho depth values are projected onto the profile in Figure 10 (location in Figure 2a). An overall decrease in crustal thickness from ~35 to ~20 km is shown, the "necking" of the crust occurring under the Arabati area (Figure 10a). We define the lower crust as the portion of crust (equivalent to a surface in cross section) between the upper/lower crust boundary and the Moho as defined above. The lower crust has an initial thickness of 20 km (from 15 to 35 km depth). When we balance the lower crust in Figure 10a (~3350 km^2) to its initial thickness of 20 km, we obtain a mean *ß* factor of ~1.4, which is lower than the mean value of ~2 obtained for the upper crust. This means that the lower crust is too thick with respect to the upper crust, or in other words, there is an excess of lower crust beneath Central Afar. In fact, in order to make the lower crustal thinning comparable to the upper crustal thinning, approximately 1850 km^2 must be subtracted from the lower crust. It may be necessary to assume that this excess crust was not present at the initial prerift stage but was instead added to the crust during rifting. Consequently, we refer to this excess lower crust as "underplating," independent of the spatial and temporal distribution of this material during rifting. At this point, a kinematically correct although unlikely solution could be obtained by adding a uniform layer of underplating in proportions that would fit the balancing, regardless of its distribution. However, this would imply that the crustal thinning crust along the whole cross section was continuous, which is inconsistent with the crustal necking inferred from receiver functions computations [*Reed et al*., 2014]. There must therefore have been a particular spatial and thus temporal distribution of the underplating beneath the Afar, related to the mode of crustal thinning. Moreover, part of this "underplated" material most likely intruded the lower crust and not only stopped beneath the original Moho.

4.3.3. Structural Style, Midcrustal Shear Zone, and Underplating

Two key observations support the presence of a flat midcrustal shear zone: (i) the uniform NE dip of tilted blocks separated by antithetic normal faulting and (ii) the wide distribution of the domino faulting style. Because the tilted blocks achieved rotation synchronously (shortly after 7 Ma) and as all of the normal faults have similar throws (generally of 100 m but occasionally up to 500 m), the crustal thinning might be expected to be distributed proportionally at depth. However, seismic receiver functions reveal a necking in the western part of the cross section. Thus, the deformation is broadly distributed at the surface (the tilted blocks occur over a ~100 km long area) and localized within a necking zone at depth. This is consistent with the presence of a top-to-west shear zone in the midcrust, which is rooted toward the west in the lower crust beneath the plateau (Figure 10b). This is also supported by detachment faulting models [*Lister and Davis*, 1989] in which thinning of the lower crust is focused on a single point, whereas extension at the surface is distributed.

Moreover, in order for the two crustal layers to be stretched by the same amount, extra lower crust needs to be assigned to the cross section. The amount of additional lower crust can be determined by comparing the

$ß_{UPPER\ CRUST}$ to the $ß_{LOWER\ CRUST}$ directly below the abrupt thinning of the upper crust, and this extra lower crust does indeed fill the "gap" left by what would be the actual thickness of the lower crust. We thus propose the existence of a flat detachment at midcrustal level beneath the Afar, which is rooted in the lower crust in the necking zone of Arabati and which corresponds to or even controls the preferential emplacement of mafic material in the zone of abrupt thinning in order to fill the voids left in the thinned crust (the shear zone in green in Figure 10b). Some of the largest faults would connect to the shear zone at depth (faults in green, Figure 10b) while crosscutting older faults (in red, Figure 10b). This mechanism might also explain the formation of the "active segments" of Tendaho and Tat'Ale, and this is supported by the findings of *Desissa et al*. [2013], who identified a wide zone of partial melting beneath Manda Hararo. We therefore propose that a more recent shear zone mechanism, analogous to the first, develops and controls the localization of deformation and magmatism at depth beneath a segment.

This interpretation relies on the observation of WSW dipping faults as being the major structures that accommodate extension on the long term. Unlike *Wolfenden et al*. [2004, 2005] farther south, we do not observe major east dipping faults, except the one bounding the Tendaho graben (Figures 1 and 2). This is either because east dipping faults have been overprinted by Miocene west dipping structures (which is unlikely) or because they never existed north of the Dessie-Bati accommodation zone [*Wolfenden et al*., 2005], which separate our study area from Wolfenden's. The major east dipping faults near Dessie (Figures 1 and 2) are located south of the accommodation zone; one of them is represented on our cross section (Figure 10). It is noteworthy that even though they control the topography south of the Dessie-Bati accommodation zone, they are not recognized as major structures in terms of crustal thinning in *Wolfenden et al*. [2005]. Therefore, such east dipping faults, if they exist in our study zone, did not act as major accommodating structures, either because they were generated during the stretching phase, or because they are minor (see Figures 5 and 10). This is compatible with the flexure we documented between the plateau and the Afar area.

It is worth noting that the wide pattern of distribution of the deformation documented in this study cannot be attributed to the presence of transfer zones. The Arabati-Chifra cross section (Figure 5) is located close to a minor transfer zone (Figures 1 and 2), where the marginal graben is slightly offset. However, the fault pattern we observed corresponds to a wide zone (more than 50 km, Figure 2) compared to the width of the transfer zone and can thus be considered as representative of the rift segment. Finally, our cross section is composite and, close to the plateau, crosses the transfer zone (the marginal graben of the cross section being south of the transfer zone and the flexure being north of it, Figures 2, 5, and 6). This has little influence on the cross section as the structural styles are quite similar on both sides.

5. Discussion

5.1. Timing of Deformation

Rifting in Central Afar from the Oligocene to the present has taken place in three main steps (Figures 11 and 12). The first tectonic event (the stretching phase) occurred at around 25 Ma, after emplacement of the Traps at 30–29 Ma and just prior to the onset of emplacement of the Miocene series at around 23 Ma, as observed in the marginal graben (Figure 12d). In Sullu Adu, the Traps were tilted to 30°E during this first tectonic phase. Thus, the stretching was distributed over a wide area (around 100 km; Figures 11 and 12d). In the southernmost part of Western Afar [*Wolfenden et al*., 2005], it has been suggested that the deformation was focused on the border faults of the marginal graben between 29 and 26 Ma (Stage 1 of *Wolfenden et al*. [2005]). In our opinion, the pre-Miocene deformation in Central Afar was more widely distributed, as suggested by the succession of grabens and tilted blocks, which have recorded 0° to 30° of bed rotation locally.

The second phase of deformation (thinning phase) (Figures 11 and 12b) occurred after the emplacement of the Miocene series, which ended at about 7 Ma (marking the end of Chifra and Finto series emplacement). In both the Arabati and Sullu Adu areas, the tilting of the Miocene series can be recognized by the absence of growth strata or by variations in thickness in the hanging wall of faults, indicating that this phase of extension occurred after emplacement of the Miocene series. Moreover, we observed that the Chifra series and Finto series were synchronous and present throughout the whole of the Miocene, from ~23 to ~7 Ma. During this period, the Miocene series appears to have been conform, although not continuous as no erosional surfaces were observed. However, it is possible that the oldest rocks of the unit are separated from the younger rocks by a paraconformity and that there were two distinct pulses of volcanism instead of one continuous,

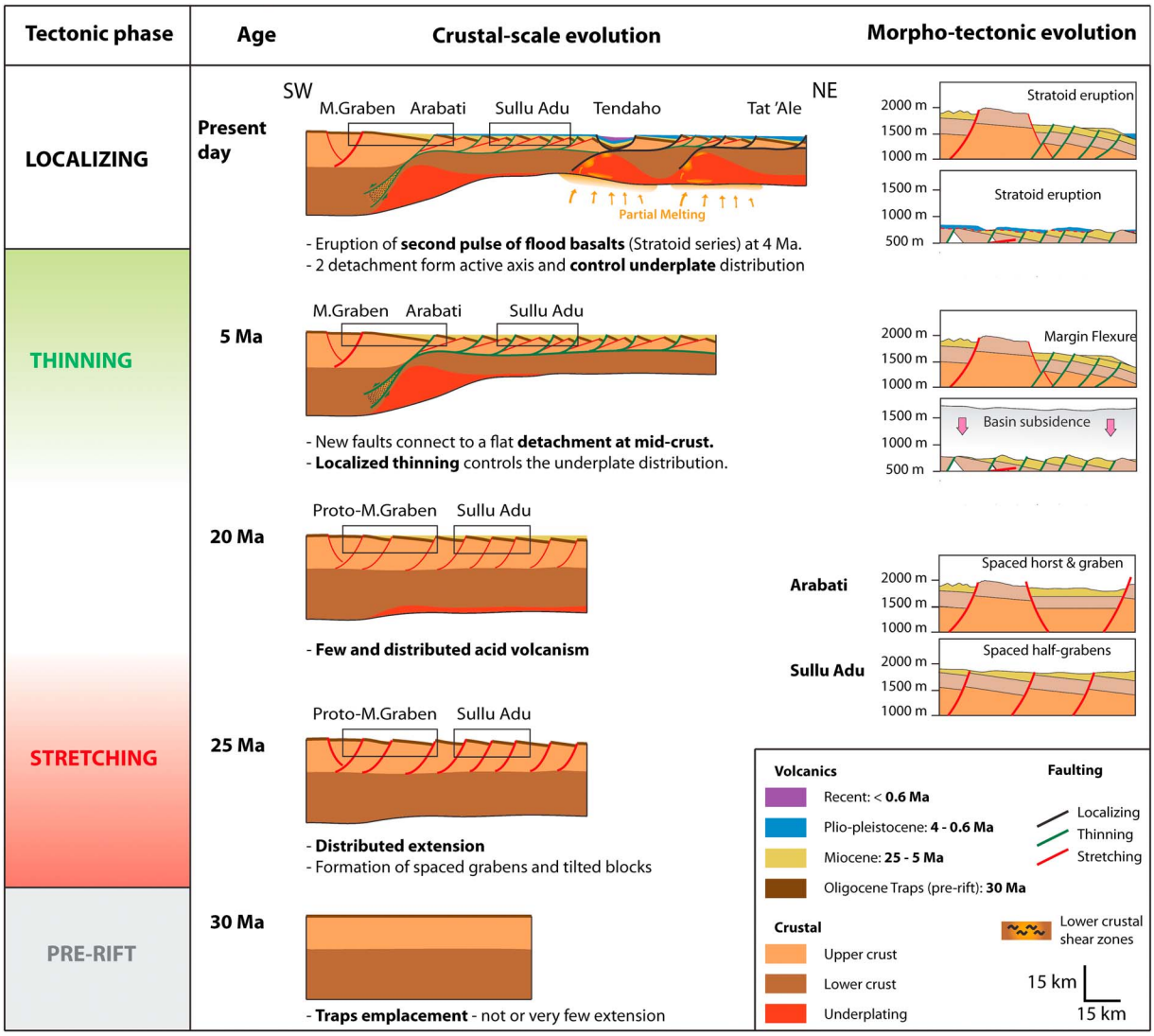

Figure 11. Volcano-tectonic evolution of Central Afar. Table figure summarizing the different tectonic phases that structured Central Afar. The Traps were emplaced at 30 Ma, during the prerift phase, probably in response to the thermal anomaly of the Afar plume. The emplacement was accompanied by no—or very little—extension. Rifting began between 30 and 25 Ma, prior to the onset of Miocene volcanism (in yellow), with a "stretching" phase. The stretching affected a wide area and was characterized by strong coupling between the brittle and ductile levels of the crust: NE dipping tilted blocks were created by the accommodation of extension on SW dipping faults. The Afar rift was already asymmetric at this point, with numerous half-grabens. The stretching phase was followed by a period of tectonic quiescence and the eruption of sparse acidic magmas (Miocene in yellow). Between ~7 and ~4 Ma, after the emplacement of the Miocene series and before the emplacement of the Stratoïd, a second tectonic phase—the "thinning phase"—occurred. During this phase, the Arabati zone underwent flexure, and the Sullu Adu zone started to subside in response to crustal thinning. The thinning phase was therefore a distributed mode of extension, during which time the crust was thinned and then partially rethickened by magmatic underplating. In our model, the normal faults of the thinning phase connect to a shear zone at depth that helped to create a necking zone in the lower crust. When tectonic activity ceased, the Stratoïd flood basalts were emplaced on top of the newly thinned Afar crust (Stratoïd volcanism from ~4 to ~0.6 Ma). This was then followed by the "localizing phase," in which the Afar remains today. Magmatic and tectonic activity is currently focused within the active segments, in our case Manda Hararo and Tat'Ale.

volume-starved series. Nevertheless, we can conclude that almost no deformation occurred in our study zone during the Miocene (Figures 11 and 12c).

In their southernmost cross sections (see in Figure 4b, profiles B to D), *Wolfenden et al.* [2005] found that magmatism and faulting shifted twice during the Miocene: an eastward jump occurring at 15 Ma and a second jump occurring at 8–7 Ma. This process produced younger basins toward the center of the rift. This model was supported by the early geological mapping of Afar of *Varet* [1978] in which the whole of the Sullu Adu ridge was interpreted as being of Dahla age (7.4 ± 0.3 Ma, Figure 2b), on the basis of a single whole rock K-Ar age of *Barberi et al.* [1975]. Our observations do not support the model of progressive strain

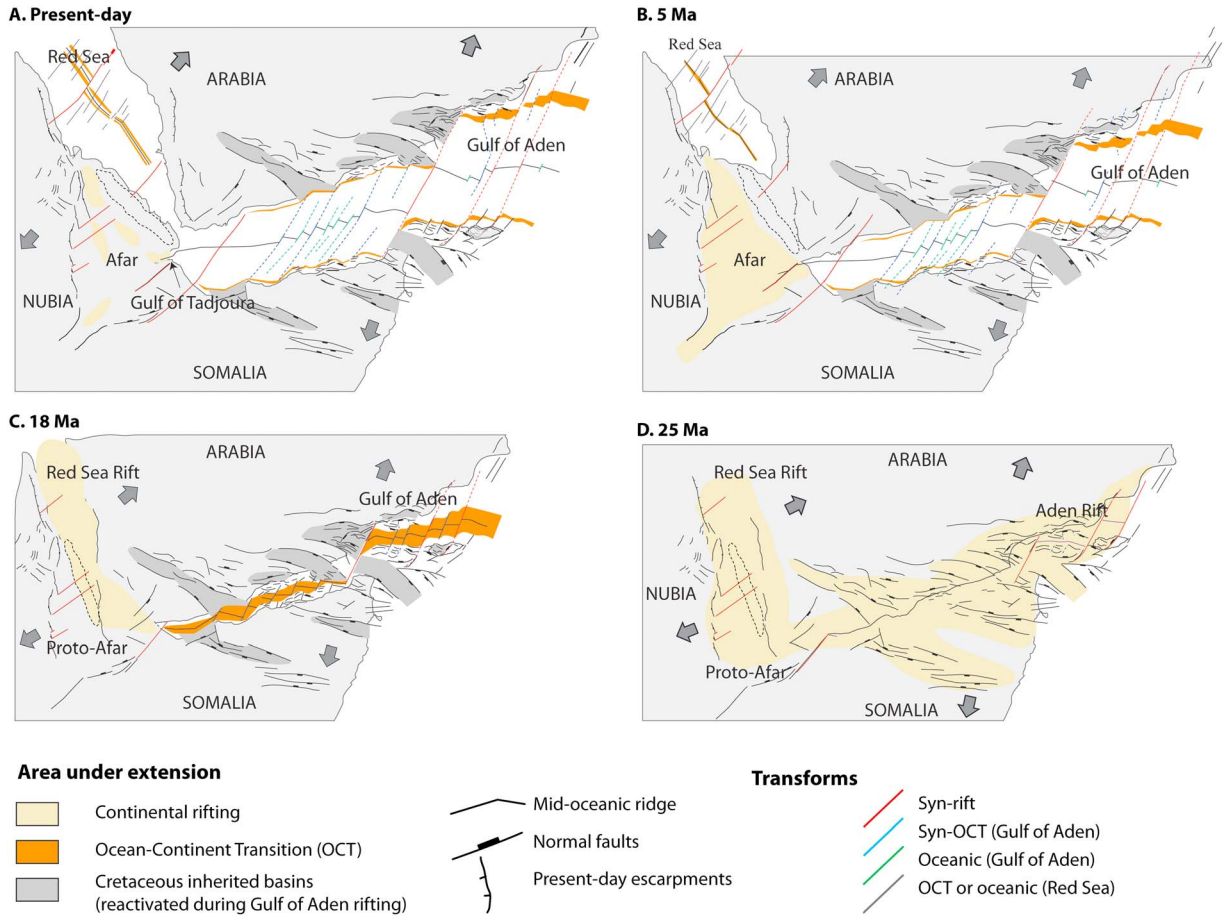

Figure 12. Geodynamic reconstruction of the movements of Nubia and Arabia during the last 25 Ma. At 25 Ma, rifting began simultaneously in the Red Sea and Afar and was already active in the Gulf of Aden. Extension in Afar was accommodated over a wide zone. At ~18 Ma, divergence in the Gulf of Aden was focused at the ocean-continent transition [e.g., *d'Acremont et al.*, 2006; *Leroy et al.*, 2012], which could have potentially triggered localization in a narrower area, possibly in the highly deformed Danakil block as no extension was recorded in Central Afar. At 5 Ma, oceanic spreading was active in both the Gulf of Aden and Red Sea. Rifting in Afar was once again widely distributed, remaining so until recently. In the present-day, divergence in Afar is taken up by localized active segments. Areas in yellow mark the zones of accommodation of divergence, whereas those in light grey mark those that have become inactive. The OCT is marked in orange, and the dark grey areas represent inherited Cretaceous rift basins that were reactivated during rifting in the Gulf of Aden. The main escarpments are shown for clarity. Structural map of the Gulf of Aden is from *Leroy et al.* [2012, and references therein]. Gulf of Aden transform timing is from *Bellahsen et al.* [2013].

migration during the Miocene [*Wolfenden et al.*, 2005] as the Miocene series are not localized in a single narrow basin, which would have been located riftward of the protomarginal graben, but are instead distributed over a large area on top of previously stretched crust (Figure 11). Our interpretation also favors widely distributed strain during the upper Miocene/lower Pliocene second phase of deformation (5 Ma, Figure 12b).

However, no extension is recorded in our study areas so there appears to have been a gap in extension during mid-Miocene times. As divergence did not stop between 23 and 7 Ma (as attested to in Gulf of Aden continental and oceanic records), we postulate that deformation took place farther to the northeast during this time, in the southern Red Sea rift or on the Danakil block.

In the Red Sea, the main phase of rifting probably began at between 27 and 22 Ma [*Omar and Steckler*, 1995; *Hugues et al.*, 1999; *Bosworth and McClay*, 2001]. The rifting may well have started earlier than this [*Omar and Steckler*, 1995], but no evidence for significant uplift and erosion is found in the sedimentary record at this time [*Bosworth et al.*, 1998]. Moreover, the ocean-continent transition in the Gulf of Aden formed at 18–20 Ma, leading to the strong localization of divergence in distal margins [*Leroy et al.*, 2004; *d'Acremont et al.*, 2006; *Leroy et al.*, 2012; *Bellahsen et al.*, 2013] (see Figure 12c). We propose that the rifting became focused in the Red Sea at around 22 Ma and that lithospheric breakup (after the OCT formation) [*Leroy et al.*, 2012] in the

Gulf of Aden at 18 Ma triggered localization of the rifting in the north, i.e., along the Red Sea/Gulf of Aden connection (Figure 12c).

From 4.0 to 1.1 Ma, the Stratoïd series erupted over a large zone at the border of Western Afar (Figure 2b), infilling the Awra basin and the more distal parts of the rift (the flat-lying Sullu Adu basalts and rhyolites, which lie horizontally above the Finto series, Figures 5, 6, and 8). Between 1.1 and 0.6 Ma, at the end of the Stratoïd emplacement (and previously included in the Stratoïd by *Varet* [1978]), a distinct mode of emplacement can be recognized [*Kidane et al*., 2003; *Lahitte et al*., 2003a]. The authors correlate these basalts with the "Gulf Basalts" Formation, which outcrops around the Gulf of Tadjoura (Figure 12a). In Central Afar, the Gulf Basalts are emplaced along massive silicic centers in the hanging wall of major west dipping normal faults that form the easternmost border of the Tendaho Graben [*Kidane et al*., 2003] (Figures 1 and 2) and in the major west dipping fault that bounds the half-graben of Tat'Ale. They are also found in association with the earliest lava flows of Manda Hararo and on top of the basaltic plateaus near Manda Inakir (Figure 2). The Gulf Basalts therefore appear to be the first geological formation in the Afar to have localized along large faults during the third phase of extension (the localizing phase) (Figure 11). After emplacement of the Gulf Basalts (ending at 0.6 Ma), a significant amount of strain, characterized by intense dyking, localized on magmatic centers [*Wright et al*., 2006; *Grandin et al*., 2010; *Pagli et al*., 2014] (Figure 11). The distribution of the Gulf basalts therefore largely corresponds to the distribution of active volcanic segments (Figures 11 and 12a).

Our interpretation therefore points toward widely distributed rifting during the Oligo-Miocene, both before and after the main flood basalt events (Oligocene traps and Pliocene Stratoïd series), although the mode of rifting switched from stretching to thinning during this period. During the Quaternary, the divergence became localized in the magmatic centers, although the process of localization may have started during emplacement of the Stratoïd series.

5.2. Extension Discrepancy and Extra Lower Crust

Our results show that the lower crust is thicker than predicted from taking into account the surface extension calculated from the cross section balancing of the upper crust. The amount of extension determined from surface balancing techniques when the amount of syn-rift lavas and sediments is excluded ($ß_{drawn} = 2.16$) in agreement with the amount calculated from the local $ß$ ($ß_{calculated} = 1.96 \pm 0.16$). This may appear to be inconsistent with a divergence model in which dyking is an important mechanism for strain accommodation. In these models, horizontal displacements are taken up by magma injection into the crust instead of displacement along normal faults [*Ebinger and Casey*, 2001; *Buck*, 2004]. Such processes are well described in the Manda Hararo active segment [e.g., *Grandin et al*., 2010] and the Main Ethiopian Rift (see the review in *Corti et al*. [2003]) and were initially inferred to explain the most recent ($<$7 Ma) formation history of Central Afar [*Wolfenden et al*., 2005] based on the observation of feeder dykes that crosscut the Dahla basalts. In our calculations using bedding dips, the dyke-accommodated divergence cannot be observed because dyke injection does not generate block rotation. Moreover, no dykes were found in either Arabati or Sullu Adu, making it difficult to directly quantify the amount of dyking-related divergence. Magma injection may play an important role in the accommodation of divergence [*Mohr*, 1989; *Buck*, 2004; *Keir et al*., 2011] and can take up to 50% of the total divergence [*Mohr*, 1989]. However, even though this process occurs in discrete segments, there is no evidence to suggest that it is significant at the scale of a whole rift. We propose instead that most of the extension is accommodated by normal faulting at the surface. This is supported, for example, by the high density of faults (1 fault/km mapped in Sullu Adu, Figure 8). However, we do not preclude an active role for magma in the accommodation of thinning and extension at depth, especially in the ductile lower crust.

If this is true, the stretching factor obtained in this study of ~2.7 is higher than those inferred from geophysics [e.g., *Hammond et al*., 2011]. It is closer to the estimation of *Eagles et al*. [2002], who provide a reconstruction of the Danakil block position with respect to Nubia and an estimation of its pole of rotation, and predicts a total extension rate of $ß > 3$ in Central and Southern Afar. However, geodynamic reconstructions such as this do not take into account the fact that the Danakil block experienced extension (Figure 12c), with bedding dips as high a 60° encountered in the prerift rocks [*Morton and Black*, 1975], and the block should not therefore be treated as a single rigid block. Further evidence comes from dykes that intrude the Jurassic limestones. Moreover, recent ($<$2 Ma) tectonic individuation of the Danakil Block (Figure 1) [*Le Gall et al*., 2011] took place with the reactivation of inherited faults, which affected the Miocene Mabla formation. Several episodes of extension may therefore have affected the block since the Oligocene.

Our structural model for the Afar rift with extra lower crust was developed in order to explain the fact that the upper crust suffered a higher amount of stretching and thinning than the lower crust. This is rarely the case along nonvolcanic rifted margins, as the amount of extension calculated from fault displacements in seismic reflection profiles (which provide an approximate estimate of the stretching factor of the upper brittle crust) is always lower than the stretching factor for the whole crust [*Driscoll and Karner*, 1998]. The likeliest explanation for this discrepancy is depth-dependent stretching [*Royden and Keen*, 1980; *Davis and Kusznir*, 2004], which may involve preferential extension of the lower crust through lower crustal flow while brittle faulting of the upper crust remains minimal [*Weinberg et al.*, 2007; *Blaich et al.*, 2008]. Alternatively, the discrepancy could be an artifact of the difficulty in determining the total amount of extension from several generations of faults (sequential faulting [*Reston*, 2005, 2007; *Ranero and Pérez-Gussinyé*, 2010]). In Afar, the problem is the opposite—there is apparently more extension in the upper crust than in the lower crust. Whether or not depth-dependent stretching due to lower crustal flow is a phenomenon at play in the Afar, our interpretation does not change. If depth-dependent stretching has been a factor in the Afar, then the lower crust would be even more thinned than the upper crust, and thus, the thick lower crust would be even more at odds and there would be even more excess lower crust. A final issue concerning lower crustal flow is the possibility of lower crustal material being transported over long distances, which would make it difficult to perform proper area balancing. It could even be argued that the lower crust may be transported out of the cross section; thus, inducing a bias in the lower crust area estimation used for balancing. However, our "weighted check" (see section 4.3.1) demonstrates that both the initials and underplated volumes have been conserved during rifting. This can be explained by the fact that we consider a relatively long cross section (250 km) so that even if material has been transported through flow, the material has stayed within the cross section and has been taken into account in our model.

5.3. Magma-Compensated Crustal Thinning During Rifting

Our interpretation of this excess lower crust is that the crust has experienced magma-compensated thinning achieved by underplating/intrusion, as is frequently observed along volcanic passive rifted margins [e.g., *Geoffroy*, 2005; *Thybo and Artemieva*, 2013] and continental magmatic rifts such as the Baikal Rift [*Thybo and Nielsen*, 2009] and the East African Rift System [*MacKenzie et al.*, 2005; *Maguire et al.*, 2006]. Magma-compensated thinning is frequently associated with the presence of high velocity bodies at the base of the lower crust. Seismic refraction profiles across the Main Ethiopian Rift (MER) have imaged a 10 km thick layer with a crustal velocity of Vp = 7.4 to 7.7 km/s [*MacKenzie et al.*, 2005; *Maguire et al.*, 2006]. In this case, the presence of mafic material that has been added to the base of the lower crust is supported by the existence of a reflective *P* wave interface above the Moho [*Maguire et al.*, 2006], which the authors interpret as the top of the high velocity body. In Central Afar, *Hammond et al.* [2011] modeled the Vp of the lower crust with receiver functions and determined values of 6.9 to 7.2 km/s. *Bastow and Keir* [2011] report lower crustal *P* wave velocities of 7.0 to 7.5 km/s beneath the Afar. Whether lower crustal layers characterized by *P* wave velocities such as those described above are of magmatic origin or whether they correspond to metamorphosed basement rocks is an issue that is still under debate [*Gernigon et al.*, 2004; *Thybo and Artemieva*, 2013]. The *P* wave velocities of the lower crust beneath the Afar range from 7.0 to 7.5 km/s [*Bastow and Keir*, 2011] and might therefore correspond to magmatic underplating. However, these values are restricted to the axial zones of the Afar and cannot alone account for magmatic underplating because the present-day elevated temperatures recorded in these segments could lower the *P* velocities. Even though these velocities are lower than in the MER, they are comparable those of other underplated bodies such as the Vøring High in the North Atlantic, which ranges from 6.9 to 7.3 km/s [*Mjelde et al.*, 2009].

Furthermore, Vp/Vs of between 1.9 and 2.2 are found in Central Afar [*Hammond et al.*, 2011] and are consistent with the presence of mafic material/injected crust. However, zones of Vp/Vs = 1.9 are found between Western Afar and Sullu Adu, which are volcanically inactive at present. This suggests that the high ratio might be better explained by mafic material whose high Vp signature would increase that of the initial continental crust. In contrast, the ratio of >2 below Tendaho and Manda Hararo would be best explained by a mixture of mafic underplating and present-day partial melting. Another important characteristic of the Central Afar crust is the presence of positive Bouguer anomalies that are accounted for by adding high density material ($d = 3000\ g/cm^3$) to the lower crust [*Tessema and Antoine*, 2004].

All of these observations strengthen a hypothesis that involves the addition of mafic material to the crust during crustal stretching. A common alternative interpretation for the underplating is that it could be either

serpentinized mantle or high-grade metamorphic rock [e.g., *Gernigon et al*., 2004]. Serpentinized mantle can display a broad range of Vp values, from 5 km/s to 7.5 km/s with Vp/Vs > 1.8 [*O'Reilly et al*., 1996] similar to those observed beneath Afar. However, serpentinization is expected when the crust has been extensively stretched and thinned [*Péron-Pinvidic and Manatschal*, 2009] thereby allowing fluids to percolate through an exhumed lithospheric mantle. Such a process seems unlikely given the ~5–10 km thickness of the upper crust [*Hammond et al*., 2011].

The data discussed above do not allow us to completely discard the hypothesis of metamorphic rocks being part of the underplating. However, the fact that a certain volume of the lower crust must have been readded to compensate for the thinning favors magmatic production of volumes that did not exist prior to extension (as metamorphism does not create new magma). In addition, Vp/Vs > 1.8 points toward an ultramafic origin for the underplating (Figure 10).

Finally, this point of view is supported by the fact that underplating of magmatic origin is usually linked to the eruption of the large volumes of basaltic and sometimes rhyolitic lavas that are characteristic of large igneous provinces across the world [*Cox*, 1980]. The volume of this underplating may be several orders of magnitude greater than the volume of the surface volcanics [*Cox*, 1993]. When a mantle source rock is partially melted and fractionated to produce basaltic liquids, some of the initial volume is retained in the form of olivine, plagioclase, and clinopyroxene-bearing cumulates. *Cox* [1980] states that only the plagioclase-bearing cumulates (gabbros) have a crustal character and are therefore associated with crustal underplating. The remaining olivine and pyroxene-rich cumulates are the ultramafic products of primary source rock differentiation and are considered to be mantle rocks. The mass fraction ratio of gabbroic cumulates over erupted liquid is at least ~0.5, which means that at least half of the volume erupted has been retained at the base of the crust. This should be considered a minimum ratio, however, because it assumes that all of the available liquid has been erupted (if this were not the case, the ratio would be higher than 0.5).

Further evidence for important volumes of underplating is the presence of rhyolitic products at the surface. *Cox* [1993] suggests that 6 to 10 times this volume may be present as cumulates in the deep crust. These cumulates could be the source rock of the rhyolites (with the rhyolites derived from the fusion of any basalt in the lower crust), or be gabbroic cumulates formed from fractional crystallization of primitive mantle liquids (of picritic composition) or could even be cumulates formed by melting and recrystallization of the basalts themselves [*Cox*, 1993]. This subtlety precludes any proper estimate of the amount of underplating because it assumes that the volume of cumulates, basalts, and rhyolites derived from original mantle source rock melting and the amount of rhyolite derived from remelting of the already differentiated basalt are both known. In our cross section, we suggest that a large volume of underplated material is stored at the base of crust (Figures 10 and 11). Given the ~1 km thick pile of mostly acidic Miocene volcanism of over ~200 km length in the cross section, plus the ~1 km thick pile of Stratoïd basalts a number of acidic centers [*Varet*, 1978] spread over 120 km (excluding the Awra plain beneath which the Stratoïd is present in the form of basaltic edifices and sparse acidic flows; Figures 2, 8, and *Coulié* [2001]), and another ~1 km of recent axial flows restricted to an area of around 20 km length, the extruded post-Traps magmas should cover an area of ~340 km^2. In contrast, the section balancing predicts a surface area of 1850 km^2 of underplated bodies (in red in Figures 10 and 11). This therefore yields an underplated/erupted area ratio of ~5.4, which is in agreement with the interpretations of *Cox* [1993].

5.4. Midcrustal Shear Zone Model

The first model of crustal attenuation by polyphase faulting (i.e., several generations of faults) for the Afar margin is from *Morton and Black* [1975]. The model was developed in order to provide constraints on how much extension the Afar floor underwent in order to facilitate Arabian-African reconstruction. The model was developed after observation of pre-Miocene rocks outcropping along Western Afar and on the Danakil Block. The original hypothesis was that the Afar floor was entirely covered with oceanic floor, and thus, the presence of silicic outcrops in the depression was problematic [*Morton and Black*, 1975]. The model was an attempt to link the thickness of the crust to the horizontal displacement deduced from bed dips. They recognized the riftward tilting blocks and postulated they were regularly spaced and then computed the effect of several generations of faults on the extension factor. For simplicity, they assumed a purely geometric model with planar faults, that none of the divergence was accommodated by dyking and that all the strain was pure shear, i.e., that deformation was progressively taken up through ductile deformation so that there was no *décollement* or major asymmetric shear zone located at depth [*Morton and Black*, 1975]. Up to here,

the approach of *Morton and Black* [1975] is similar to our own (see section 3). However, in using the seismic refraction profiles of *Berckhemer et al*. [1975], *Mohr* [1983] argued in favor of a décollement mechanism, through which the upper brittle crust is decoupled from the ductile lower crust. Differential thinning between the upper crustal layer (Vp = 6.0–6.1 km/s), which thins from 12 km under Addis Ababa to 4 km under Mille, and the lower crustal layer (Vp = 6.6–6.7), which thins from 30 km under Addis Ababa to 18 km under Mille, certainly occurs (Figure 2). Thus, the upper crust has a *ß* of ~3, whereas the lower crust a *ß* of ~1.7. However, contrary to the remarks of *Mohr* [1983], second-generation faults are indeed observed [*Rooney et al*., 2013]. This last observation supports our model of polyphase faulting. Thus, the model of *Morton and Black* [1975] lacks a feature that could explain both the necking of the crust at depth and the spatial distribution of the tilted blocks at the surface. As suggested by *Mohr* [1983], a shear zone (or décollement) at midcrustal level might be a possible solution. Midcrustal shear zones have already been directly observed in the northernmost part of Afar by *Ghebreab and Talbot* [2000] on the Eritrean Plateaus and in the neighboring Gulf of Zula. In particular, they observed tilted blocks that had been dissected by seaward dipping normal faults rooted in an inferred top-to-the-east shear zone. According to the authors, the extension exploited an inherited Pan-African low-angle fabric which represented an incipient detachment zone. During a second phase of extension, landward normal faults crosscut the preexisting detachment at the surface in a domino fashion and are rooted in an inferred second detachment at depth with top-to-the-west orientation. The Eritrean escarpment was therefore proposed to consist of a monoclinal flexure due to the second detachment. The seaward dipping blocks of Eritrea were interpreted by *Ghebreab and Talbot* [2000] to be the equivalent of onshore SDR observed at the Disko flexure in west Greenland [*Geoffroy et al*., 1998].

The models of SDR formation above a midcrustal shear zone are consistent with our interpretations in Central Afar. In our model, we infer the presence of a shear zone in order to fit the deep crustal necking to the widely distributed surface extension so that our cross section is balanced. There is however an important difference between our interpretation and the "classical" view of syn-tectonic SDR formation. Our observations show that the main stretching and thinning episodes took place in between magmatic pulses (Figure 11). We documented (1) an Oligocene prerift magmatic pulse (the Trap Basalts) followed by a stretching phase, (2) a protracted Miocene acidic magmatic phase followed by an episode of thinning and underplating, and (3) a second major magmatic pulse (the Pliocene Stratoïd), later followed by a localizing phase. Consequently, the eruption of the Stratoïd basalts, which are a characteristic feature of the wide and thick Central Afar segment, occurred over a crustal layer that had previously been intensively thinned and subsequently rethickened. In our chronology, the magmatic compensation for the thinning is sequential: we did not observe any syn-volcanic thinning or stretching. Thus, from a chronological point of view, the crust is "rethickened" after an extension phase. This may appear to be at odds with observations made at other onshore volcanic passive margins, such as the SE Afar rift in Djibouti [*Geoffroy et al*., 2014]. Here syn-tectonic prisms of 8 to 2 Ma age (stage partly intermediate between Figures 12b and 12c) are thought to be controlled by rollover faults that are rooted in a detachment at depth that controls the location of future breakup. It is important to specify that this is a recent feature, younger than 2 Ma, linked to the propagation of the Aden ridge into Afar [*Geoffroy et al*., 2014]. Features such as the rollover faults may be hidden below the volcanics of the Manda Hararo magmatic center (Figures 1 and 2). Although we do not directly observe this kind of detachment system, our model contains the same kind of feature beneath the Manda Hararo axis, with a breakaway located at Affara Dara, where the prerift rocks outcrop (Figures 1, 2, and 10b).

In our midcrustal shear zone model, the location of detachments rooted in the lower crust (i.e., the locus of maximum thinning) exerts a strong control on the distribution of underplating. Extra lower crust is added at the footwalls of detachments where the lower crust is thinnest, i.e., where the pressure gradients are most favorable for ascending mafic material. Comparable mechanisms have been described for megamullions at slow-spreading ridges, where core complex-like detachments are interpreted as nonconservative faults because magmatic material is continuously stored at the base of the detachment footwall and are preferentially underplated, like plutons, during amagmatic periods [*Dick et al*., 2008]. These faults are thus termed "plutonic growth faults" by the authors.

5.5. A "Magmatic Wide Rift" During the Mio-Pliocene

GPS measurements in the MER and Central Afar have revealed that despite relative localization of strain in the active volcanic segments, the distribution of deformation was accommodated within a zone that widens

gradually from the Southern MER (~6 km) to the Afar (175 km) [*Kogan et al*., 2012]. Deformation in Afar is thus distributed over a length that exceeds the lithosphere thickness. This corresponds to the definition of a "wide rift" [*Buck*, 1991; *Brun*, 1999]. Wide rifting has occurred in natural extensional settings such as the Basin and Range province [*Lister and Davis*, 1989]. *Kogan et al*. [2012] related the increasing size of the actively extending zone from the MER to Afar to a reduction in the integrated lithosphere strength, as modeled by *Stamps et al*. [2010], and to the thinning of the lithospheric mantle under Afar [*Pasyanos et al*., 2009]. They suggested that the disappearance of the strong lithospheric mantle enhanced the gradual widening of the zone of strain accommodation. The presence of hot mantle beneath Afar was reported in the early work of *Makris and Ginzburg* [1987] and later in *Bastow et al*. [2008] (and references therein). More recently, *Stork et al*. [2013] and *Corbeau et al*. [2014] showed the presence of a low velocity mantle (*P* waves velocities of 7.2 ± 0.4 km/s) beneath a zone encompassing the western flexure to Manda Hararo. This may indicate a weakening of the uppermost mantle and, since low lithospheric mantle strength due to mantle thinning can trigger delocalization [e.g., *Sokoutis et al*., 2007], could thus explain the delocalizing pattern observed by *Kogan et al*. [2012]. In contrast, *Reed et al*. [2014] found that crustal thinning in the area adjacent to the Tendaho Graben was not focused under the graben but was instead quite diffuse. They suggested that most of the extension was diffusely accommodated by the ductile lower crust and that the lower crust is decoupled from the brittle upper crust, a parameter that may enhance delocalizing [*Davis and Kusznir*, 2004; *Reed et al*., 2014].

We propose that this wide rift strain pattern, characteristic of magmatically weakened lithosphere and crust, was already present in early Miocene times, i.e., during the early rifting. This means that the mantle was already hot at the beginning of rifting, still under the influence of the mantle thermal anomaly that was responsible for the eruption of the Traps at 30 Ma. Our aim is not to discuss the provenance of such a thermal anomaly (e.g., a mantle plume) but to highlight the fact that the temperature effect and the subsequent mantle thermal erosion and weakening has had an effect on the structural style of Afar since the early history of rifting, and that this effect is recorded in the distribution of Miocene and Pliocene faults and volcanic sequences.

In Iceland, rollover structures have formed during the last 12 Ma. These tectono-magmatic structures were underlain by shallow magma chambers at different places within a large zone about 200 km wide and were triggered by the decoupling of the upper crust from the lower crust [*Bourgeois et al*., 2005]. Moreover, this strain distribution tends to disappear away from the sustained temperature anomaly of the mantle, i.e., the Icelandic plume. This is consistent with our model of a midcrustal detachment above the thermal anomaly, this detachment being rooted in the lower crust in a more localized fashion beneath the Plateau, away from the thermal anomaly.

The novelty of our model is that it combines this "magmatically enhanced wide rifting" mode with localized necking at depth. It does not therefore oppose a mechanism of dyke injection that localizes strain in the rift center into narrow magmatic segments [e.g., *Ebinger*, 2005, and references therein]. It instead suggests that such processes may have been active during earlier rifting and distributed the strain over a wide zone.

5.6. Segmentation and SDR Formation

As described in *Bastow and Keir* [2011], the wide and thick Central Afar rift segment and the narrow and thin Northern Afar Erta'Ale segment experienced different amounts of magma eruption in relation to stretching and thinning. For Central Afar, we have shown in this study that extension has been accommodated over a wide zone as it has in other volcanic settings with a magmatic wide rifting mode, such as Iceland. Furthermore, Central Afar has experienced intense volcanism with the eruption of the Stratoïd flood basalts at 4 Ma. In northern Afar (Erta'Ale segment), the crust has been thinned to ~15 km and the Stratoïd series is absent. Instead, a Miocene sedimentary infill has accumulated in the subsiding basin. Between these two provinces, a NE-SW transfer zone has developed (Figure 1).

Along the North and South Atlantic margins, the emplacement of the SDR occurred in close relationship with major syn-rift transfer faults, and thus, the observed along-strike variation in breakup-related magmatism appears to have been controlled by the rift segmentation [*Franke et al*., 2007; *Elliott and Parson*, 2008]. Numerical simulations in *Koopmann et al*. [2014] show that a delay in the opening of a rift segment bound by a transfer fault zone can explain the difference in SDR volume on either side of the transfer fault zone. Furthermore numerical modeling [*Armitage et al*., 2009] has shown that SDR volumes observed in the Atlantic required not only a thermal anomaly, but also a previously thinned lithosphere in order to be erupted.

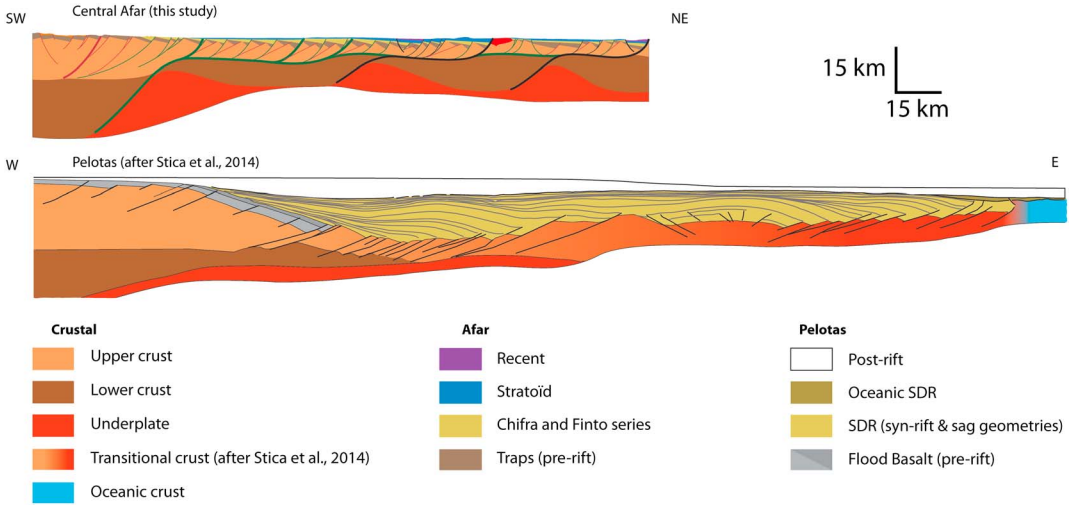

Figure 13. Comparison of the Central Afar half-rift presented in this study and an interpreted seismic line of the Pelotas basin (modified from *Stica et al.* [2014]).

This suggests that the presence of the Stratoïd in Central Afar and its absence in northern Afar is closely related to the two rift segment morphologies. Although we cannot tell whether the segmentation influenced the magmatism or if the major transfer zones were the result of the distribution of preexisting partial melting sources in the mantle, it appears that the two are strongly linked. *Bastow and Keir* [2011] stated that the northern Afar is closest to break up because it is thinner, however, we suggest in this study that breakup in Afar is not necessarily a function of the apparent thickness of the crust. The northern Afar has not experienced the same amount of magmatism and underplating as Central Afar. Furthermore, the mantle temperature anomaly was most likely lower in northern Afar than in Central Afar, and the mode of rifting appears to have been different as a result.

5.7. Comparison With Volcanic Passive Margins

The model presented here has several implications for the formation of volcanic margins. In Figure 13, we compare our Central Afar cross section to a section of the Pelotas margin in the South Atlantic [*Stica et al.*, 2014]. The thinning of SDR formation at the Pelotas margin, though unclear, appears to have been syn-rift, coeval with the first rifting phase of thinning and followed by a phase of sag-like accommodation of lava weight [*Stica et al.*, 2014]. The overall thickness of the SDR is several tens of kilometers, whereas in Central Afar it is only few km thick (Figures 5, 6, and 8). This is likely due to the fact that Central Afar has not yet reached the breakup stage. If magma decompression is enhanced by a thin lithosphere, as suggested by the eruption of the Stratoïd above a thin crust (Figures 10 and 11), then the complete removal of the initial crustal thickness should provoke another, breakup-related, pulse of magmatism which would cover up the preexisting tilted blocks. In our view, SDR development is controlled by two parameters: (1) the intensity of magma decompression, which is probably enhanced by thinning of the crust (with maximum thinning experienced during breakup; see section 5.6, above), and (2) mantle temperature. *Rooney et al.* [2012] showed that the Ethiopian Large Igneous Province (LIP) has a lower mantle potential temperature (Tp) than any other LIP. A Tp anomaly of +170°C characterizes the Oligocene flood basalt, whereas the Tp anomaly of <10 Myr old lavas in Djibouti is only +140°C [*Rooney et al.*, 2012]. The recent lavas at Manda Hararo exhibit a Tp anomaly of +150°C [*Ferguson et al.*, 2013]. Although hotter than normal asthenospheric mantle [Tp = 1350 ± 50°C, *Herzberg et al.*, 2007], the Tp recorded in the Afar lavas are still some 100°C lower than in the North Atlantic Province [*Rooney et al.*, 2012]. Even though crustal thinning has been shown to be the primary control on massive SDR emplacement along the North Atlantic margins [*Armitage et al.*, 2009], it is likely that a low Tp would have had an effect on the volumes of magma produced and erupted. In Afar, we suggest that the Stratoïd to recent lava series are equivalent to SDR or proto-SDR (blue and purple units in Figures 1, 2, 8, and 10) as they thicken toward and into the active magmatic segment (i.e., the rift center). These (proto)-SDR are emplaced over an already thinned and intruded/underplated crust.

An important question raised by examining the Pelotas margin in Figure 13 is the temporal relationship between the SDR emplacement and the first oceanic crust. Toward the ocean, the most recent layers of the SDR fan lie on oceanic crust, which means that the youngest part of the SDR fan is postbreakup (or syn-breakup), emplaced after (or during) the formation of the first oceanic crust (Figure 13). This implies that breakup sometimes occurs during the SDR emplacement, some of the layers being syn-rift, others being postrift. In our schematic cross section (Figure 13), it appears that the place where the lower crust is the youngest (i.e., thinned and rethickened by underplating during rifting) corresponds to the thinnest part of the upper crust, where most of the material is erupted volcanics. In this particular view, the breakup consists of the complete removal of the upper crust, which would then be replaced by volcanic material. Successive rethickening by mafic material would then modify the lower crust in the same way that the initial prerift lower crust was thinned to 0 km and then replaced by new syn-rift accreted lower crust, analogous to the transitional crust described in many models [e.g., *Menzies et al*., 2002; *White et al*., 2008; *Franke*, 2013]. We suggest that in this type of magma-rich environment, breakup can be defined as the complete removal of the upper crust, marking a lateral transition from "continental upper crust and continental lower crust" to "surface volcanics and newly accreted gabbroic lower crust", the latter is constituting the continent-ocean transition. This would be consistent with the model of magma-assisted extensional growth presented in the study of *Quirk et al*. [2014]. Here, a high quality seismic line from East Greenland was used to observe the transitional crust beneath the SDR. The SDR were observed in a 50 km wide band between the continental slope and the oceanic crust, underlain by a narrow necking zone. The transitional SDR-bearing crust (identified using magnetic and gravimetric profiles) is composed of around 4 km of volcanics forming the SDR fans, 4 to 6 km of faulted midcrust, and 2 to 5.5 km of lower crust, which correlates with mafic underplating toward the continent [*Quirk et al*., 2014]. The SDR fans begin in the hanging wall of a major landward dipping fault. The continental upper crust disappears on the footwall of this fault. The fault then flattens and is rooted in the lower crust. The authors interpret this ~160 km long structure as being the last syn-rift fault as it marks the outer limit of the continental crust, and they therefore referred to it as "Breakup Fault" [*Quirk et al*., 2014]. The outer limit of the transitional SDR domain is marked by a second major fault—referred to as "Ocean Continent Boundary" that separates the SDR from "normally" structured oceanic crust [*Quirk et al*., 2014]. According to their observations and to the magnetic and gravimetric inversion data of *Voss et al*. [2009], the lower crust of the transitional domain has the same composition as both the continental underplating and the oceanic crust.

Despite the similarities between Central Afar and the present-day volcanic passive margins of Pelotas and East Greenland, there are some important differences. The first is that the length of the half-margin appears to be narrower for the two present-day rifted margins. The transitional crust zone is also narrow in East Greenland (~50 km [*Quirk et al*., 2014]), which infers localized rifting. This is consistent with volcanic passive margin formation models that predict a narrow margin as a result of localized extension [e.g., *Callot et al*., 2001, 2002, and references therein]. In these models, the rapid necking of a strong, four-layered lithosphere is achieved by incorporating a weak zone in the mantle, corresponding to a thermal anomaly [*Callot et al*., 2001]. These thermal anomalies, or soft points [*Geoffroy*, 2001], are assumed to be persistent zones of localized partial melting in the mantle that act as local rheological weaknesses. They favor the localization of the breakup zone and drive the segmentation of the future margin [*Callot et al*., 2002]. However, the models do not consider the possibility that a broad zone of the mantle may be anomalously hot, which would have an effect on the distribution of the deformation (see section 5.5). Although our results do not allow us to predict the future zone of breakup or the geometry of any transitional domain, the widely distributed strain in Central Afar "half-margin" might be attributed to rheological modification due to the absence of "normal" brittle lithospheric mantle and an elevated Moho temperature.

Another difference is the size of the underplating beneath the Pelotas margin compared to Central Afar (Figure 13). In Pelotas, the underplated layer seems to be too thin to compensate for the amount of erupted SDR. One possible reason for this is that the required volume of mafic material left over after SDR differentiation is hard to estimate. In section 5.3, estimation of cumulate volumes was seen to be closely tied to the composition of extruded lavas. If the minimum underplating/erupted lava ratio of ~0.5 of *Cox* [1993] is correct for primitive basalts, then the amount of underplating present below the Pelotas margin in Figure 13 may well be correct. However, if there are more-evolved lavas, such as rhyolites, present in the SDR, then this ratio should be considerably higher [*Cox*, 1993]. If so, the thinness of the underplated layer might instead be

explained by a ductile nature of the underplating. In this case, lateral mass movements enhanced by ductile flow could displace the underplating and thus lead to an apparent deficit in the volume budget along strike.

6. Conclusions

In this contribution, we have refined the volcanic stratigraphy of Central Afar and remapped certain key areas along a transect that stretches from the Ethiopian plateau to the Manda Hararo active rift axis. We show that extension was accommodated over a wide zone during the early Miocene rifting and that extension remained diffuse until the recent formation of an active volcanic axis (<1 Ma). We also demonstrate that the tectono-magmatic evolution of the Central Afar was marked by two flood basalt pulses (at 30 and 4 Ma) each followed by a tectonic phase (stretching, thinning, and localizing). Long periods of tectonic quiescence are characterized by "starved" volcanism with the emplacement of rhyolitic series during the Miocene (23–7 Ma). This apparent gap in the extension record implies that extension must have been at play elsewhere on the Danakil block (and southern red Sea), which can no longer be considered as an undeformed, steady microcontinent.

The crust has experienced much more thinning than is usually documented by geophysical studies in this area. Our restorations suggest that thinning of the Afar crust has been compensated for by magma intrusion and underplating. We argue in favor of a shear zone at midcrustal levels with a top-to-west sense of shear on which landward dipping continental faults are rooted. Such a structure explains both the distributed fault pattern in the upper crust and the localization of crustal thinning into a narrow necking zone at depth. The presence of crustal underplating is predicted by our restorations. This underplating would be distributed in the lower crust but mostly below the deep root of the detachments. Moreover, the predicted volume of underplated material is consistent with the volume of the lava series erupted at the surface.

Once the crust had been sufficiently thinned (although its thickness was partially maintained by magma addition), the Stratoïd flood basalt pulse occurred, which was possibly analogous to SDR. We have called this particular tectono-magmatic style of rifting "magmatic wide rifting", and we link it to the effect of mantle temperature and magma on the lithospheric rheology. In the case of Central Afar, both factors prevent localization of deformation: thermal attenuation and weakening of the lithospheric mantle coupled with weak and thick lower crust during extension led to a distributed mode of rifting.

The difference between the wide, magma-rich, thick crust Central Afar segment, and the narrow, thin, and relatively magma-poor Northern Afar Erta'Ale segment is probably due to differences in magma supply. Both segments are probably close to breakup and apparent crustal thickness cannot be used to predict the location and timing of breakup.

The implications of our findings are that volcanic rifted margins are not necessarily narrow and that the wide rift mode can occur and be maintained during most of the history of rifting until the area proceeds to break up. Eruption of large magma volumes (such as SDR) is not necessarily synchronous with the lithospheric thinning, but may rather intrude into and erupt over an already thinned lithosphere.

Acknowledgments

The various structural and radiometric data used to produce the maps and cross section in this article are all presented in the figures and tables. This work was financially supported by the "Actions Marges" program and by TOTAL. For their help on the field, we would like to thank the Afar local government and the Ministry of Mines of Semara. The authors thank Bouchaïb Tibari (CRPG) for technical assistance with (U-Th-Sm)/He analyses, Gilles Peltzer (UCLA) for providing Landsat imagery, Alain Rabaute (UPMC) for his help with the SIG mapping, and Cécile Doubre (EOST) for useful discussions. We acknowledge Claudio Faccenna and Derek Keir for editorial handling along with Julie Rowland and one anonymous reviewer for their critical reading and comments, which were of great help in improving the quality of the manuscript. We finally warmly thank Alice Williams for providing many useful corrections to the English. This is CRPG contribution 2404.

References

Acocella, V., B. Abebe, T. Korme, and F. Barberi (2008), Structure of Tendaho Graben and Manda Hararo Rift: Implications for the evolution of the southern Red Sea propagator in Central Afar, *Tectonics*, *27*, TC4016, doi:10.1029/2007TC002236.

Ahmed, A., C. Tiberi, S. Leroy, G. W. Stuart, D. Keir, J. Sholan, K. Khanbari, I. Al-Ganad, and C. Basuyau (2013), Crustal structure of the rifted volcanic margins and uplifted plateau of Western Yemen from receiver function analysis, *Geophys. J. Int.*, *193*(3), 1673–1690, doi:10.1093/gji/ggt072.

Anderson, D. L. (1994), Superplumes or supercontinents?, *Geology*, *22*(1), 39, doi:10.1130/0091-7613(1994)022<0039:SOS>2.3.CO;2.

Anderson, D. L. (2005), Large igneous provinces, delamination, and fertile mantle, *Elements*, *1*(5), 271–275.

Armitage, J. J., T. J. Henstock, T. A. Minshull, and J. R. Hopper (2009), Lithospheric controls on melt production during continental breakup at slow rates of extension: Application to the North Atlantic, *Geochem. Geophys. Geosyst.*, *10*, Q06018, doi:10.1029/2009GC002404.

ArRajehi, A., et al. (2010), Geodetic constraints on present-day motion of the Arabian Plate: Implications for Red Sea and Gulf of Aden rifting, *Tectonics*, *29*, TC3011, doi:10.1029/2009TC002482.

Audin, L., X. Quidelleur, E. Coulié, V. Courtillot, S. Gilder, I. Manighetti, P.-Y. Gillot, P. Tapponnier, and T. Kidane (2004), Palaeomagnetism and K-Ar and 40Ar/39Ar ages in the Ali Sabieh area (Republic of Djibouti and Ethiopia): Constraints on the mechanism of Aden ridge propagation into southeastern Afar during the last 10 Myr, *Geophys. J. Int.*, *158*(1), 327–345.

Ayalew, D., and S. A. Gibson (2009), Head-to-tail transition of the Afar mantle plume: Geochemical evidence from a Miocene bimodal basalt–rhyolite succession in the Ethiopian Large Igneous Province, *Lithos*, *112*(3–4), 461–476, doi:10.1016/j.lithos.2009.04.005.

Baker, J. A., L. Snee, and M. Menzies (1996a), A brief Oligocene period of flood volcanism in Yemen: Implications for the duration and rate of continental flood volcanism at the Afro-Arabian triple junction, *Earth Planet. Sci. Lett.*, *138*(1), 39–55.

Baker, J. A., M. F. Thirlwall, and M. A. Menzies (1996b), Sr-Nd-Pb isotopic and trace element evidence for crustal contamination of plume-derived flood basalts: Oligocene flood volcanism in western Yemen, *Geochim. Cosmochim. Acta*, *60*(14), 2559–2581.
Ballmer, M. D., J. van Hunen, G. Ito, P. J. Tackley, and T. A. Bianco (2007), Non-hotspot volcano chains originating from small-scale sublithospheric convection, *Geophys. Res. Lett.*, *34*, L23310, doi:10.1029/2007GL031636.
Barberi, F., G. Ferrara, R. Santacroce, and J. Varet (1975), Structural evolution of the Afar triple junction, in *Afar Depression of Ethiopia*, vol. 1, pp. 38–54, Schweizerbart, Stuttgart, Germany.
Bastow, I. D., and D. Keir (2011), The protracted development of the continent–ocean transition in Afar, *Nat. Geosci.*, *4*(4), 248–250, doi:10.1038/ngeo1095.
Bastow, I. D., A. A. Nyblade, G. W. Stuart, T. O. Rooney, and M. H. Benoit (2008), Upper mantle seismic structure beneath the Ethiopian hot spot: Rifting at the edge of the African low-velocity anomaly, *Geochem. Geophys. Geosyst.*, *9*, Q12022, doi:10.1029/2008GC002107.
Bellahsen, N., C. Faccenna, F. Funiciello, J. M. Daniel, and L. Jolivet (2003), Why did Arabia separate from Africa? Insights from 3-D laboratory experiments, *Earth Planet. Sci. Lett.*, *216*(3), 365–381, doi:10.1016/S0012-821X(03)00516-8.
Bellahsen, N., L. Husson, J. Autin, S. Leroy, and E. d'Acremont (2013), The effect of thermal weakening and buoyancy forces on rift localization: Field evidences from the Gulf of Aden oblique rifting, *Tectonophysics*, *607*, 80–97, doi:10.1016/j.tecto.2013.05.042.
Benoit, M. H., A. A. Nyblade, and J. C. VanDecar (2006), Upper mantle *P*-wave speed variations beneath Ethiopia and the origin of the Afar hotspot, *Geology*, *34*(5), 329–332.
Berckhemer, H., B. Baier, H. Bartelsen, A. Behle, H. Burkhardt, H. Gebrande, J. Makris, H. Menzel, H. Miller, and R. Vees (1975), Deep seismic soundings in the Afar region and on the highland of Ethiopia, in *Afar Depression of Ethiopia, Proceedings of an International Symposium on the Afar Region and Related Rift Problems, Bad Bergzabern, F.R. Germany, April 1–6, 1974*, vol. 1, edited by A. Pilger and A. Rösler, pp. 89–107, Schweizerbart, Stuttgart, Germany.
Berktold, A., V. Haak, and G. Angenheister (1975), Magnetotelluric measurements in the Afar area, in *Afar Depression of Ethiopia, Proceedings of an International Symposium on the Afar Region and Related Rift Problems, Bad Bergzabern, F.R. Germany, April 1–6, 1974*, vol. 1, edited by A. Pilger and A. Rösler, pp. 66–79, Schweizerbart, Stuttgart, Germany.
Blaich, O. A., F. Tsikalas, and J. I. Faleide (2008), Northeastern Brazilian margin: Regional tectonic evolution based on integrated analysis of seismic reflection and potential field data and modelling, *Tectonophysics*, *458*(1–4), 51–67, doi:10.1016/j.tecto.2008.02.011.
Bosworth, W., and K. McClay (2001), Structural and stratigraphic evolution of the Gulf of Suez rift, Egypt: A synthesis, *Mem. Mus. Natl. Hist. Nat.*, *186*, 567–606.
Bosworth, W., P. Crevello, R. D. Winn Jr., and J. Steinmetz (1998), Structure, sedimentation, and basin dynamics during rifting of the Gulf of Suez and north-western Red Sea, in *Sedimentation and Tectonics in Rift Basins Red Sea: Gulf of Aden*, pp. 77–96, Springer, Netherlands.
Bourgeois, O., O. Dauteuil, and E. Hallot (2005), Rifting above a mantle plume: Structure and development of the Iceland Plateau, *Geodin. Acta*, *18*(1), 59–80.
Bridges, D. L., K. Mickus, S. S. Gao, M. G. Abdelsalam, and A. Alemu (2012), Magnetic stripes of a transitional continental rift in Afar, *Geology*, *40*(3), 203–206, doi:10.1130/G32697.1.
Brun, J. P. (1999), Narrow rifts versus wide rifts: Inferences for the mechanics of rifting from laboratory experiments, *Philos. Trans. R. Soc. A*, *357*, 695–712.
Buck, W. R. (1991), Modes of continental lithospheric extension, *J. Geophys. Res.*, *96*(B12), 20,161–20,178, doi:10.1029/91JB01485.
Buck, W. R. (2004), Consequences of asthenospheric variability on continental rifting, in *Rheology and Deformation of the Lithosphere at Continental Margins*, vol. 62, pp. 1–30, Columbia Univ. Press.
Buck, W. R. (2006), The role of magma in the development of the Afro-Arabian Rift System, *Geol. Soc. London Spec. Publ.*, *259*(1), 43–54.
Callot, J. P., C. Grigné, L. Geoffroy, and J. P. Brun (2001), Development of volcanic passive margins: Two-dimensional laboratory models, *Tectonics*, *20*(1), 148–159, doi:10.1029/2000TC900030.
Callot, J.-P., L. Geoffroy, and J.-P. Brun (2002), Development of volcanic passive margins: Three-dimensional laboratory models, *Tectonics*, *21*(6), 1052, doi:10.1029/2001TC901019.
Casey, M., C. Ebinger, D. Keir, R. Gloaguen, and F. Mohamed (2006), Strain accommodation in transitional rifts: Extension by magma intrusion and faulting in Ethiopian rift magmatic segments, *Geol. Soc. London Spec. Publ.*, *259*, 143–163, doi:10.1144/GSL.SP.2006.259.01.13.
Coffin, M. F., and O. Eldholm (1994), Large igneous provinces: Crustal structure, dimensions, and external consequences, *Rev. Geophys.*, *32*(1), 1–36, doi:10.1029/93RG02508.
Corbeau, J., et al. (2014), Uppermost mantle velocity from Pn tomography in the Gulf of Aden, *Geosphere*, *10*(5), 958–968.
Corti, G. (2009), Continental rift evolution: From rift initiation to incipient break-up in the Main Ethiopian Rift, East Africa, *Earth Sci. Rev.*, *96*(1–2), 1–53, doi:10.1016/j.earscirev.2009.06.005.
Corti, G., M. Bonini, S. Conticelli, F. Innocenti, P. Manetti, and D. Sokoutis (2003), Analogue modelling of continental extension: A review focused on the relations between the patterns of deformation and the presence of magma, *Earth Sci. Rev.*, *63*(3-4), 169–247, doi:10.1016/S0012-8252(03)00035-7.
Coulié, E. (2001), Chronologie $^{40}Ar/^{39}Ar$ et K/Ar de la déchirure continentale en Afar depuis 30 Ma, PhD, Université Paris Sud.
Coulié, E., X. Quidelleur, P.-Y. Gillot, V. Courtillot, J.-C. Lefèvre, and S. Chiesa (2003), Comparative K–Ar and Ar/Ar dating of Ethiopian and Yemenite Oligocene volcanism: Implications for timing and duration of the Ethiopian traps, *Earth Planet. Sci. Lett.*, *206*(3), 477–492.
Courtillot, V., C. Jaupart, I. Manighetti, P. Tapponnier, and J. Besse (1999), On causal links between flood basalts and continental breakup, *Earth Planet. Sci. Lett.*, *166*(3), 177–195.
Cox, K. G. (1980), A model for flood basalt vulcanism, *J. Petrol.*, *21*(4), 629–650.
Cox, K. G. (1993), Continental magmatic underplating, *Philos. Trans. R. Soc. London A*, *342*, 155–166.
Craig, T. J., J. A. Jackson, K. Priestley, and D. McKenzie (2011), Earthquake distribution patterns in Africa: Their relationship to variations in lithospheric and geological structure, and their rheological implications, *Geophys. J. Int.*, *185*(1), 403–434, doi:10.1111/j.1365-246X.2011.04950.x.
d'Acremont, E., S. Leroy, M. Maia, P. Patriat, M.-O. Beslier, N. Bellahsen, M. Fournier, and P. Gente (2006), Structure and evolution of the eastern Gulf of Aden: Insights from magnetic and gravity data (Encens-Sheba MD117 cruise), *Geophys. J. Int.*, *165*(3), 786–803, doi:10.1111/j.1365-246X.2006.02950.x.
d'Acremont, E., S. Leroy, M. Maia, P. Gente, and J. Autin (2010), Volcanism, jump and propagation on the Sheba ridge, eastern Gulf of Aden: Segmentation evolution and implications for oceanic accretion processes, *Geophys. J. Int.*, *180*(2), 535–551, doi:10.1111/j.1365-246X.2009.04448.x.
Daradich, A., J. X. Mitrovica, R. N. Pysklywec, S. D. Willett, and A. M. Forte (2003), Mantle flow, dynamic topography, and rift-flank uplift of Arabia, *Geology*, *31*(10), 901–904.

Davis, M., and N. J. Kusznir (2004), Depth-dependent lithospheric stretching at rifted continental margins, in *Proceedings of NSF Rifted Margins Theoretical Institute*, pp. 92–136, Columbia Univ. Press.
Desissa, M., N. E. Johnson, K. A. Whaler, S. Hautot, S. Fisseha, and G. J. K. Dawes (2013), A mantle magma reservoir beneath an incipient mid-ocean ridge in Afar, Ethiopia, *Nat. Geosci.*, *6*(10), 861–865, doi:10.1038/ngeo1925.
Dick, H. J. B., M. A. Tivey, and B. E. Tucholke (2008), Plutonic foundation of a slow-spreading ridge segment: Oceanic core complex at Kane Megamullion, 23°30′N, 45°20′W: Plutonic foundation of a slow-spreading ridge segment, *Geochem. Geophys. Geosyst.*, *9*, Q05014, doi:10.1029/2007GC001645.
Driscoll, N. W., and G. D. Karner (1998), Lower crustal extension across the Northern Camarvon basin, Australia: Evidence for an eastward dipping detachment, *J. Geophys. Res.*, *103*(B3), 4975–4991, doi:10.1029/97JB03295.
Dugda, M. T., A. A. Nyblade, J. Julia, C. A. Langston, C. J. Ammon, and S. Simiyu (2005), Crustal structure in Ethiopia and Kenya from receiver function analysis: Implications for rift development in eastern Africa, *J. Geophys. Res.*, *110*, B01303, doi:10.1029/2004JB003065.
Dugda, M. T., A. A. Nyblade, and J. Julia (2007), Thin lithosphere beneath the Ethiopian Plateau revealed by a joint inversion of Rayleigh wave group velocities and receiver functions, *J. Geophys. Res.*, *112*, B08305, doi:10.1029/2006JB004918.
Eagles, G., R. Gloaguen, and C. Ebinger (2002), Kinematics of the Danakil microplate, *Earth Planet. Sci. Lett.*, *203*(2), 607–620.
Ebinger, C. (2005), Continental break-up: The East African perspective, *Astron. Geophys.*, *46*(2), 2–16.
Ebinger, C., and N. J. Hayward (1996), Soft plates and hot spots: Views from Afar, *J. Geophys. Res.*, *101*(B10), 21,859–21,876, doi:10.1029/96JB02118.
Ebinger, C. J., and M. Casey (2001), Continental breakup in magmatic provinces: An Ethiopian example, *Geology*, *29*(6), 527–530.
Ebinger, C. J., J. van Wijk, and D. Keir (2013), The time scales of continental rifting: Implications for global processes, *Geol. Soc. Am. Spec. Publ.*, *500*, 371–396.
Elliott, G. M., and L. M. Parson (2008), Influence of margin segmentation upon the break-up of the Hatton Bank rifted margin, NE Atlantic, *Tectonophysics*, *457*(3–4), 161–176, doi:10.1016/j.tecto.2008.06.008.
Faccenna, C., T. W. Becker, L. Jolivet, and M. Keskin (2013), Mantle convection in the Middle East: Reconciling Afar upwelling, Arabia indentation and Aegean trench rollback, *Earth Planet. Sci. Lett.*, *375*, 254–269, doi:10.1016/j.epsl.2013.05.043.
Ferguson, D. J., J. Maclennan, I. D. Bastow, D. M. Pyle, S. M. Jones, D. Keir, J. D. Blundy, T. Plank, and G. Yirgu (2013), Melting during late-stage rifting in Afar is hot and deep, *Nature*, *499*(7456), 70–73, doi:10.1038/nature12292.
Franke, D. (2013), Rifting, lithosphere breakup and volcanism: Comparison of magma-poor and volcanic rifted margins, *Mar. Pet. Geol.*, *43*, 63–87, doi:10.1016/j.marpetgeo.2012.11.003.
Franke, D., S. Neben, S. Ladage, B. Schreckenberger, and K. Hinz (2007), Margin segmentation and volcano-tectonic architecture along the volcanic margin off Argentina/Uruguay, South Atlantic, *Mar. Geol.*, *244*(1–4), 46–67, doi:10.1016/j.margeo.2007.06.009.
Geoffroy, L. (2001), The structure of volcanic margins: Some problematics from the North-Atlantic/Labrador–Baffin system, *Mar. Pet. Geol.*, *18*(4), 463–469.
Geoffroy, L. (2005), Volcanic passive margins, *C. R. Geosci.*, *337*(16), 1395–1408, doi:10.1016/j.crte.2005.10.006.
Geoffroy, L., J. P. Gélard, C. Lepvrier, and P. Olivier (1998), The coastal flexure of Disko (West Greenland), onshore expression of the "oblique reflectors," *J. Geol. Soc.*, *155*(3), 463–473.
Geoffroy, L., B. Le Gall, M. A. Daoud, and M. Jalludin (2014), Flip-flop detachment tectonics at nascent passive margins in SE Afar, *J. Geol. Soc.*, doi:10.1144/jgs2013-135.
Gernigon, L., J.-C. Ringenbach, S. Planke, and B. Le Gall (2004), Deep structures and breakup along volcanic rifted margins: Insights from integrated studies along the outer Vøring Basin (Norway), *Mar. Pet. Geol.*, *21*(3), 363–372, doi:10.1016/j.marpetgeo.2004.01.005.
Ghebreab, W., and C. J. Talbot (2000), Red Sea extension influenced by Pan-African tectonic grain in eastern Eritrea, *J. Struct. Geol.*, *22*(7), 931–946.
Gillot, P.-Y., and Y. Cornette (1986), The Cassignol technique for potassium—Argon dating, precision and accuracy: Examples from the Late Pleistocene to recent volcanics from southern Italy, *Chem. Geol.*, *59*, 205–222.
Grandin, R., A. Socquet, E. Jacques, N. Mazzoni, J.-B. de Chabalier, and G. C. P. King (2010), Sequence of rifting in Afar, Manda-Hararo rift, Ethiopia, 2005–2009: Time-space evolution and interactions between dikes from interferometric synthetic aperture radar and static stress change modeling, *J. Geophys. Res.*, *115*, B10413, doi:10.1029/2009JB000815.
Hammond, J. O. S., J.-M. Kendall, G. W. Stuart, D. Keir, C. Ebinger, A. Ayele, and M. Belachew (2011), The nature of the crust beneath the Afar triple junction: Evidence from receiver functions, *Geochem. Geophys. Geosyst.*, *12*, Q12004, doi:10.1029/2011GC003738.
Hammond, J. O. S., et al. (2013), Mantle upwelling and initiation of rift segmentation beneath the Afar Depression, *Geology*, *41*(6), 635–638, doi:10.1130/G33925.1.
Harding, D. J., C. J. Ebinger, and J. Heirtzler (1990), Lateral displacements on intersecting fault sets of the Afar depression, *Eos Trans. AGU*, *71*, 617.
Hayward, N. J., and C. J. Ebinger (1996), Variations in the along-axis segmentation of the Afar Rift system, *Tectonics*, *15*(2), 244–257, doi:10.1029/95TC02292.
Herzberg, C., P. D. Asimow, N. Arndt, Y. Niu, C. M. Lesher, J. G. Fitton, M. J. Cheadle, and A. D. Saunders (2007), Temperatures in ambient mantle and plumes: Constraints from basalts, picrites, and komatiites, *Geochem. Geophys. Geosyst.*, *8*, Q02006, doi:10.1029/2006GC001390.
Hinz, K. (1981), *A Hypothesis on Terrestrial Catastrophes Wedges of Very Thick Oceanward Dipping Layers Beneath Passive Continental Margins: Their Origin and Pleoenvironmental Significance*, Schweizerbart, Stuttgart, Germany.
Hofmann, C., V. Courtillot, G. Feraud, P. Rochette, G. Yirgu, E. Ketefo, and R. Pik (1997), Timing of the Ethiopian flood basalt event and implications for plume birth and global change, *Nature*, *389*(6653), 838–841.
Holbrook, W. S., H. C. Larsen, J. Korenaga, T. Dahl-Jensen, I. D. Reid, P. B. Kelemen, J. R. Hopper, G. M. Kent, D. Lizarralde, and S. Bernstein (2001), Mantle thermal structure and active upwelling during continental breakup in the North Atlantic, *Earth Planet. Sci. Lett.*, *190*(3), 251–266.
Hugues, G. W., D. Perincek, D. J. Grainger, A.-J. Abu-Bshait, and A.-R. M. Jarad (1999), Lithostratigraphy and depositional history of part of the Midyan region, northwestern Saudi Arabia, *GeoArabia*, *4*, 503–541.
Huismans, R. S., Y. Y. Podladchikov, and S. Cloetingh (2001), Transition from passive to active rifting: Relative importance of asthenospheric doming and passive extension of the lithosphere, *J. Geophys. Res.*, *106*(B6), 11,271–11,291, doi:10.1029/2000JB900424.
Keir, D., C. Pagli, I. D. Bastow, and A. Ayele (2011), The magma-assisted removal of Arabia in Afar: Evidence from dike injection in the Ethiopian rift captured using InSAR and seismicity, *Tectonics*, *30*(2), doi:10.1029/2010TC002785.
Keir, D., I. D. Bastow, C. Pagli, and E. L. Chambers (2013), The development of extension and magmatism in the Red Sea rift of Afar, *Tectonophysics*, *607*, 98–114, doi:10.1016/j.tecto.2012.10.015.
Kidane, T., V. Courtillot, I. Manighetti, L. Audin, P. Lahitte, X. Quidelleur, P.-Y. Gillot, Y. Gallet, J. Carlut, and T. Haile (2003), New paleomagnetic and geochronologic results from Ethiopian Afar: Block rotations linked to rift overlap and propagation and determination of a ~2 Ma reference pole for stable Africa, *J. Geophys. Res.*, *108*(B2), 2102, doi:10.1029/2001JB000645.

Kieffer, B., et al. (2004), Flood and shield basalts from Ethiopia: Magmas from the African superswell, *J. Petrol.*, *45*(4), 793–834, doi:10.1093/petrology/egg112.
Kogan, L., S. Fisseha, R. Bendick, R. Reilinger, S. McClusky, R. King, and T. Solomon (2012), Lithospheric strength and strain localization in continental extension from observations of the East African Rift, *J. Geophys. Res.*, *117*, B03402, doi:10.1029/2011JB008516.
Koopmann, H., S. Brune, D. Franke, and S. Breuer (2014), Linking rift propagation barriers to excess magmatism at volcanic rifted margins, *Geology*, doi:10.1130/G36085.1.
Korostelev, F., et al. (2014), Crustal and upper mantle structure beneath south-western margin of the Arabian Peninsula from teleseismic tomography, *Geochem. Geophys. Geosyst.*, *15*, 2850–2864, doi:10.1002/2014GC005316.
Kunz, K., H. Kreuzer, and P. Müller (1975), Potassium-Argon age determinations of the Trap basalt of the south-eastern part of the Afar Rift, in *Afar Depression of Ethiopia*, vol. 1, pp. 370–374, Schweizerbart, Stuttgart, Germany.
Lahitte, P., E. Coulié, N. Mercier, T. Kidane, and P.-Y. Gillot (2001), Chronologie K–Ar et TL du volcanisme aux extrémités sud du propagateur mer Rouge en Afar depuis 300 ka, *C. R. Acad. Sci., Ser. IIa: Sci. Terre Planetes*, *332*(1), 13–20.
Lahitte, P., P.-Y. Gillot, T. Kidane, V. Courtillot, and A. Bekele (2003a), New age constraints on the timing of volcanism in central Afar, in the presence of propagating rifts, *J. Geophys. Res.*, *108*(B2), 2123, doi:10.1029/2001JB001689.
Lahitte, P., P.-Y. Gillot, and V. Courtillot (2003b), Silicic central volcanoes as precursors to rift propagation: The Afar case, *Earth Planet. Sci. Lett.*, *207*(1–4), 103–116, doi:10.1016/S0012-821X(02)01130-5.
Le Bas, M. J. (1987), Ultra-alkaline magmatism with or without rifting, *Tectonophysics*, *143*(1), 75–84.
Le Gall, B. (2014), Carte Géologique de la République de Djibouti, 1/200 000, CCGM, Paris.
Le Gall, B., M. A. Daoud, J. Rolet, and N. M. Egueh (2011), Large-scale flexuring and antithetic extensional faulting along a nascent plate boundary in the SE Afar rift: Structure of a nascent plate boundary in SE Afar, *Terra Nova*, *23*(6), 416–420, doi:10.1111/j.1365-3121.2011.01029.x.
Le Pichon, X., and J.-C. Sibuet (1981), Passive margins: A model of formation, *J. Geophys. Res.*, *86*(B5), 3708–3720, doi:10.1029/JB086iB05p03708.
Leroy, S., et al. (2004), From rifting to spreading in the eastern Gulf of Aden: A geophysical survey of a young oceanic basin from margin to margin, *Terra Nova*, *16*(4), 185–192, doi:10.1111/j.1365-3121.2004.00550.x.
Leroy, S., et al. (2012), From rifting to oceanic spreading in the Gulf of Aden: A synthesis, *Arabian J. Geosci.*, *5*(5), 859–901, doi:10.1007/s12517-011-0475-4.
Li, C., R. D. van der Hilst, E. R. Engdahl, and S. Burdick (2008), A new global model for P wave speed variations in Earth's mantle, *Geochem. Geophys. Geosyst.*, *9*, Q05018, doi:10.1029/2007GC001806.
Lister, G. S., and G. A. Davis (1989), The origin of metamorphic core complexes and detachment faults formed during Tertiary continental extension in the northern Colorado River region, *USA, J. Struct. Geol.*, *11*(1), 65–94.
Mackenzie, G. D., H. Thybo, and P. K. H. Maguire (2005), Crustal velocity structure across the Main Ethiopian Rift: Results from two-dimensional wide-angle seismic modelling, *Geophys. J. Int.*, *162*(3), 994–1006, doi:10.1111/j.1365-246X.2005.02710.x.
Maguire, P. K. H., et al. (2006), Crustal structure of the northern Main Ethiopian Rift from the EAGLE controlled-source survey: A snapshot of incipient lithospheric break-up, *Spec. Publ. Geol. Soc. London*, *259*, 269.
Makris, J., and A. Ginzburg (1987), The Afar Depression: Transition between continental rifting and sea-floor spreading, *Tectonophysics*, *141*(1), 199–214.
Manighetti, I., P. Tapponnier, P. Y. Gillot, E. Jacques, V. Courtillot, R. Armijo, J. C. Ruegg, and G. King (1998), Propagation of rifting along the Arabia-Somalia plate boundary: Into Afar, *J. Geophys. Res.*, *103*(B3), 4947–4974, doi:10.1029/97JB02758.
Marty, B., R. Pik, and Y. Gezahegn (1996), Helium isotopic variations in Ethiopian plume lavas: Nature of magmatic sources and limit on lower mantle contribution, *Earth Planet. Sci. Lett.*, *144*(1), 223–237.
McClusky, S., et al. (2010), Kinematics of the southern Red Sea-Afar Triple Junction and implications for plate dynamics, *Geophys. Res. Lett.*, *37*, L05301, doi:10.1029/2009GL041127.
McKenzie, D. (1978), Some remarks on the development of sedimentary basins, *Earth Planet. Sci. Lett.*, *40*(1), 25–32.
Medynski, S., et al. (2013), Controls on magmatic cycles and development of rift topography of the Manda Hararo segment (Afar, Ethiopia): Insights from cosmogenic ^{3}He investigation of landscape evolution, *Earth Planet. Sci. Lett.*, *367*, 133–145, doi:10.1016/j.epsl.2013.02.006.
Medynski, S., et al. (2015), Stability of rift axis magma reservoirs: Spatial and temporal evolution of magma supply in the Dabbahu rift segment (Afar, Ethiopia) over the past 30 kyr, *Earth Planet. Sci. Lett.*, *409*, 278–289, doi:10.1016/j.epsl.2014.11.002.
Menzies, M. A., S. L. Klemperer, C. J. Ebinger, and J. Baker (2002), Characteristics of volcanic rifted margins, *Geol. Soc. Am. Spec. Pap.*, *362*, 1–14.
Mjelde, R., J. I. Faleide, A. J. Breivik, and T. Raum (2009), Lower crustal composition and crustal lineaments on the Vøring Margin, NE Atlantic: A review, *Tectonophysics*, *472*(1–4), 183–193, doi:10.1016/j.tecto.2008.04.018.
Mohr, P. (1978), Afar, *Annu. Rev. Earth Planet. Sci.*, *6*, 145–172.
Mohr, P. (1983), The Morton-Black hypothesis for the thinning of continental crust—Revisited in western Afar, *Tectonophysics*, *94*(1), 509–528.
Mohr, P. (1989), Nature of the crust under Afar: New igneous, not thinned continental, *Tectonophysics*, *167*(1), 1–11.
Morton, W. H., and R. Black (1975), Crustal attenuation in Afar, in *Afar Depression of Ethiopia, Proceedings of an International Symposium on the Afar Region and Related Rift Problems, Bad Bergzabern, F.R. Germany, April 1–6, 1974*, vol. 1, edited by A. Pilger and A. Rösler, pp. 55–61, Schweizerbart, Stuttgart, Germany.
Mutter, J. C., M. Talwani, and P. L. Stoffa (1982), Origin of seaward-dipping reflectors in oceanic crust off the Norwegian margin by "subaerial sea-floor spreading", *Geology*, *10*(7), 353–357.
Nikishin, A. M., P. A. Ziegler, D. Abbott, M.-F. Brunet, and S. Cloetingh (2002), Permo–Triassic intraplate magmatism and rifting in Eurasia: Implications for mantle plumes and mantle dynamics, *Tectonophysics*, *351*(1), 3–39.
Nobile, A., C. Pagli, D. Keir, T. J. Wright, A. Ayele, J. Ruch, and V. Acocella (2012), Dike-fault interaction during the 2004 Dallol intrusion at the northern edge of the Erta Ale Ridge (Afar, Ethiopia), *Geophys. Res. Lett.*, *39*, L19305, doi:10.1029/2012GL053152.
Omar, G. I., and M. S. Steckler (1995), Fission track evidence on the initial rifting of the Red Sea: Two pulses, no propagation, *Science*, *270*(5240), 1341–1344, doi:10.1126/science.270.5240.1341.
O'Reilly, B. M., F. Hauser, A. B. Jacob, and P. M. Shannon (1996), The lithosphere below the Rockall Trough: Wide-angle seismic evidence for extensive serpentinisation, *Tectonophysics*, *255*(1), 1–23.
Pagli, C., T. J. Wright, C. J. Ebinger, S.-H. Yun, J. R. Cann, T. Barnie, and A. Ayele (2012), Shallow axial magma chamber at the slow-spreading Erta Ale Ridge, *Nat. Geosci.*, *5*(4), 284–288, doi:10.1038/ngeo1414.
Pagli, C., H. Wang, T. J. Wright, E. Calais, and E. Lewi (2014), Current plate boundary deformation of the Afar rift from a 3-D velocity field inversion of InSAR and GPS: Current Afar plate boundary deformation, *J. Geophys. Res. Solid Earth*, *119*, 8562–8575, doi:10.1002/2014JB011391.
Pasyanos, M. E., W. R. Walter, and E. M. Matzel (2009), A simultaneous multiphase approach to determine P-wave and S-wave attenuation of the crust and upper mantle, *Bull. Seismol. Soc. Am.*, *99*(6), 3314–3325.

Pérez-Gussinyé, M., M. Metois, M. Fernández, J. Vergés, J. Fullea, and A. R. Lowry (2009), Effective elastic thickness of Africa and its relationship to other proxies for lithospheric structure and surface tectonics, *Earth Planet. Sci. Lett.*, *287*(1–2), 152–167, doi:10.1016/j.epsl.2009.08.004.

Péron-Pinvidic, G., and G. Manatschal (2009), The final rifting evolution at deep magma-poor passive margins from Iberia-Newfoundland: A new point of view, *Int. J. Earth Sci.*, *98*(7), 1581–1597, doi:10.1007/s00531-008-0337-9.

Péron-Pinvidic, G., G. Manatschal, and P. T. Osmundsen (2013), Structural comparison of archetypal Atlantic rifted margins: A review of observations and concepts, *Mar. Pet. Geol.*, *43*, 21–47, doi:10.1016/j.marpetgeo.2013.02.002.

Pik, R., C. Deniel, C. Coulon, G. Yirgu, C. Hofmann, and D. Ayalew (1998), The northwestern Ethiopian Plateau flood basalts: Classification and spatial distribution of magma types, *J. Volcanol. Geotherm. Res.*, *81*(1), 91–111.

Pik, R., C. Deniel, C. Coulon, G. Yirgu, and B. Marty (1999), Isotopic and trace element signatures of Ethiopian flood basalts: Evidence for plume–lithosphere interactions, *Geochim. Cosmochim. Acta*, *63*(15), 2263–2279.

Pik, R., B. Marty, J. Carignan, and J. Lavé (2003), Stability of the Upper Nile drainage network (Ethiopia) deduced from (U–Th)/He thermochronometry: Implications for uplift and erosion of the Afar plume dome, *Earth Planet. Sci. Lett.*, *215*(1–2), 73–88, doi:10.1016/S0012-821X(03)00457-6.

Pik, R., B. Marty, and D. R. Hilton (2006), How many mantle plumes in Africa? The geochemical point of view, *Chem. Geol.*, *226*(3-4), 100–114, doi:10.1016/j.chemgeo.2005.09.016.

Pik, R., B. Marty, J. Carignan, G. Yirgu, and T. Ayalew (2008), Timing of East African Rift development in southern Ethiopia: Implication for mantle plume activity and evolution of topography, *Geology*, *36*(2), 167–170.

Quirk, D. G., A. Shakerley, and M. J. Howe (2014), A mechanism for construction of volcanic rifted margins during continental breakup, *Geology*, *42*(12), 1079–1082, doi:10.1130/G35974.1.

Ranero, C. R., and M. Pérez-Gussinyé (2010), Sequential faulting explains the asymmetry and extension discrepancy of conjugate margins, *Nature*, *468*(7321), 294–299, doi:10.1038/nature09520.

Redfield, T. F., W. H. Wheeler, and M. Often (2003), A kinematic model for the development of the Afar Depression and its paleogeographic implications, *Earth Planet. Sci. Lett.*, *216*(3), 383–398, doi:10.1016/S0012-821X(03)00488-6.

Reed, C. A., S. Almadani, S. S. Gao, A. A. Elsheikh, S. Cherie, M. G. Abdelsalam, A. K. Thurmond, and K. H. Liu (2014), Receiver function constraints on crustal seismic velocities and partial melting beneath the Red Sea rift and adjacent regions, Afar Depression, *J. Geophys. Res. Solid Earth*, *119*, 2138–2152, doi:10.1002/2013JB010719.

Reston, T. (2007), Extension discrepancy at North Atlantic nonvolcanic rifted margins: Depth-dependent stretching or unrecognized faulting?, *Geology*, *35*(4), 367, doi:10.1130/G23213A.1.

Reston, T. J. (2005), Polyphase faulting during the development of the west Galicia rifted margin, *Earth Planet. Sci. Lett.*, *237*(3–4), 561–576, doi:10.1016/j.epsl.2005.06.019.

Ritsema, J., and R. M. Allen (2003), The elusive mantle plume, *Earth Planet. Sci. Lett.*, *207*(1–4), 1–12, doi:10.1016/S0012-821X(02)01093-2.

Ritsema, J., A. Deuss, H. J. van Heijst, and J. H. Woodhouse (2011), S40RTS: A degree-40 shear-velocity model for the mantle from new Rayleigh wave dispersion, teleseismic traveltime and normal-mode splitting function measurements, *Geophys. J. Int.*, *184*(3), 1223–1236, doi:10.1111/j.1365-246X.2010.04884.x.

Rochette, P., E. Tamrat, G. Féraud, R. Pik, V. Courtillot, E. Ketefo, C. Coulon, C. Hoffmann, D. Vandamme, and G. Yirgu (1998), Magnetostratigraphy and timing of the Oligocene Ethiopian traps, *Earth Planet. Sci. Lett.*, *164*(3), 497–510.

Rooney, T. O., C. Herzberg, and I. D. Bastow (2012), Elevated mantle temperature beneath East Africa, *Geology*, *40*(1), 27–30.

Rooney, T. O., P. Mohr, L. Dosso, and C. Hall (2013), Geochemical evidence of mantle reservoir evolution during progressive rifting along the western Afar margin, *Geochim. Cosmochim. Acta*, *102*, 65–88, doi:10.1016/j.gca.2012.08.019.

Rooney, T. O., I. D. Bastow, D. Keir, F. Mazzarini, E. Movsesian, E. B. Grosfils, J. R. Zimbelman, M. S. Ramsey, D. Ayalew, and G. Yirgu (2014a), The protracted development of focused magmatic intrusion during continental rifting, *Tectonics*, *33*, 875–897, doi:10.1002/2013TC003514.

Rooney, T. O., W. R. Nelson, L. Dosso, T. Furman, and B. Hanan (2014b), The role of continental lithosphere metasomes in the production of HIMU-like magmatism on the northeast African and Arabian plates, *Geology*, *42*(5), 419–422, doi:10.1130/G35216.1.

Royden, L., and C. E. Keen (1980), Rifting process and thermal evolution of the continental margin of eastern Canada determined from subsidence curves, *Earth Planet. Sci. Lett.*, *51*(2), 343–361.

Rychert, C. A., J. O. S. Hammond, N. Harmon, J. Michael Kendall, D. Keir, C. Ebinger, I. D. Bastow, A. Ayele, M. Belachew, and G. Stuart (2012), Volcanism in the Afar Rift sustained by decompression melting with minimal plume influence, *Nat. Geosci.*, *5*(6), 406–409, doi:10.1038/ngeo1455.

Sengör, A. M., and K. Burke (1978), Relative timing of rifting and volcanism on Earth and its tectonic implications, *Geophys. Res. Lett.*, *5*(6), 419–421, doi:10.1029/GL005i006p00419.

Simmons, N. A., A. M. Forte, and S. P. Grand (2007), Thermochemical structure and dynamics of the African superplume, *Geophys. Res. Lett.*, *34*, L02301, doi:10.1029/2006GL028009.

Sokoutis, D., G. Corti, M. Bonini, J. Pierre Brun, S. Cloetingh, T. Mauduit, and P. Manetti (2007), Modeling the extension of heterogeneous hot lithosphere, *Tectonophysics*, *444*(1–4), 63–79, doi:10.1016/j.tecto.2007.08.012.

Stamps, D. S., L. M. Flesch, and E. Calais (2010), Lithospheric buoyancy forces in Africa from a thin sheet approach, *Int. J. Earth Sci.*, *99*(7), 1525–1533, doi:10.1007/s00531-010-0533-2.

Stica, J. M., P. V. Zalán, and A. L. Ferrari (2014), The evolution of rifting on the volcanic margin of the Pelotas Basin and the contextualization of the Paraná–Etendeka LIP in the separation of Gondwana in the South Atlantic, *Mar. Pet. Geol.*, *50*, 1–21, doi:10.1016/j.marpetgeo.2013.10.015.

Stork, A. L., G. W. Stuart, C. M. Henderson, D. Keir, and J. O. S. Hammond (2013), Uppermost mantle (Pn) velocity model for the Afar region, Ethiopia: An insight into rifting processes, *Geophys. J. Int.*, *193*(1), 321–328, doi:10.1093/gji/ggs106.

Tessema, A., and L. A. G. Antoine (2004), Processing and interpretation of the gravity field of the East African Rift: Implication for crustal extension, *Tectonophysics*, *394*(1–2), 87–110, doi:10.1016/j.tecto.2004.07.057.

Thybo, H., and I. M. Artemieva (2013), Moho and magmatic underplating in continental lithosphere, *Tectonophysics*, *609*, 605–619, doi:10.1016/j.tecto.2013.05.032.

Thybo, H., and C. A. Nielsen (2009), Magma-compensated crustal thinning in continental rift zones, *Nature*, *457*(7231), 873–876, doi:10.1038/nature07688.

Ukstins, I. A., P. R. Renne, E. Wolfenden, J. Baker, D. Ayalew, and M. Menzies (2002), Matching conjugate volcanic rifted margins: $^{40}Ar/^{39}Ar$ chrono-stratigraphy of pre- and syn-rift bimodal flood volcanism in Ethiopia and Yemen, *Earth Planet. Sci. Lett.*, *198*(3), 289–306.

Van Wijk, J. W., R. S. Huismans, M. Ter Voorde, and S. Cloetingh (2001), Melt generation at volcanic continental margins: No need for a mantle plume?, *Geophys. Res. Lett.*, *28*(20), 3995–3998, doi:10.1029/2000GL012848.

Varet, J. (1978), Geology of central and southern Afar (Ethiopia and Djibouti Republic), map and report, 124 pp.

Voss, M., M. C. Schmidt-Aursch, and W. Jokat (2009), Variations in magmatic processes along the East Greenland volcanic margin, *Geophys. J. Int.*, *177*(2), 755–782, doi:10.1111/j.1365-246X.2009.04077.x.

Weinberg, R. F., K. Regenauer-Lieb, and G. Rosenbaum (2007), Mantle detachment faults and the breakup of cold continental lithosphere, *Geology*, *35*(11), 1035, doi:10.1130/G23918A.1.

White, R. S., et al. (2008), Lower-crustal intrusion on the North Atlantic continental margin, *Nature*, *452*(7186), 460–464, doi:10.1038/nature06687.

Wolfenden, E., C. Ebinger, G. Yirgu, A. Deino, and D. Ayalew (2004), Evolution of the northern Main Ethiopian rift: Birth of a triple junction, *Earth Planet. Sci. Lett.*, *224*(1–2), 213–228, doi:10.1016/j.epsl.2004.04.022.

Wolfenden, E., C. Ebinger, Y. Gezahegn, P. R. Renne, and S. P. Kelley (2005), Evolution of a volcanic rifted margin: Southern Red Sea, Ethiopia, *Geol. Soc. Am. Bull.*, *117*(7–8), 846–864, doi:10.1130/B25516.1.

Wright, T. J., C. Ebinger, J. Biggs, A. Ayele, G. Yirgu, D. Keir, and A. Stork (2006), Magma-maintained rift segmentation at continental rupture in the 2005 Afar dyking episode, *Nature*, *442*(7100), 291–294, doi:10.1038/nature04978.

Zanettin, B., and E. Justin-Visentin (1975), Tectonical and volcanological evolution of the western Afar margin (Ethiopia), in *Afar Depression of Ethiopia, Proceedings of an International Symposium on the Afar Region and Related Rift Problems, Bad Bergzabern, F.R. Germany, April 1–6, 1974*, vol. 1, edited by A. Pilger and A. Rösler, pp. 300–309, Schweizerbart, Stuttgart, Germany.

Ziegler, P. A., and S. Cloetingh (2004), Dynamic processes controlling evolution of rifted basins, *Earth Sci. Rev.*, *61*(1–2), 1–50, doi:10.1016/S0012-8252(03)00041-2.

Ziegler, P. A., S. Cloetingh, R. Guiraud, and G. M. Stampfli (2001), Peri-Tethyan platforms: Constraints on dynamics of rifting and basin inversion, *Mem. Mus. Natl. Hist. Nat.*, *186*, 9–49.

Zumbo, V., G. Féraud, P. Vellutini, P. Piguet, and J. Vincent (1995), First 40Ar39Ar dating on early pliocene to plio-pleistocene magmatic events of the Afar—Republic of Djibouti, *J. Volcanol. Geotherm. Res.*, *65*(3), 281–295.